

University of Alabama in Huntsville

**LOUIS**

---

Theses

UAH Electronic Theses and Dissertations

---

2018

## Preliminary trajectory design using nuclear fusion propulsion for rendezvous missions to Jupiter and Saturn

Saroj Kumar

Follow this and additional works at: <https://louis.uah.edu/uah-theses>

---

### Recommended Citation

Kumar, Saroj, "Preliminary trajectory design using nuclear fusion propulsion for rendezvous missions to Jupiter and Saturn" (2018). *Theses*. 633.  
<https://louis.uah.edu/uah-theses/633>

This Thesis is brought to you for free and open access by the UAH Electronic Theses and Dissertations at LOUIS. It has been accepted for inclusion in Theses by an authorized administrator of LOUIS.

**PRELIMINARY TRAJECTORY DESIGN USING NUCLEAR FUSION  
PROPULSION FOR RENDEZVOUS MISSIONS TO JUPITER AND SATURN**

by

**Saroj Kumar**

A Thesis

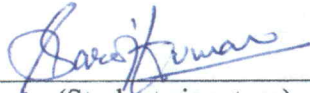
**Submitted in partial fulfillment of the requirements  
For the degree of Master of Science Aerospace Systems Engineering  
in  
The Department of Mechanical and Aerospace Engineering  
of  
The School of Graduate Studies  
of  
The University of Alabama in Huntsville**

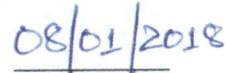
**HUNTSVILLE, ALABAMA**

**2018**



In presenting this thesis in partial fulfillment of the requirements for a master's degree from The University of Alabama in Huntsville, I agree that the Library of this University shall make it freely available for inspection. I further agree that permission for extensive copying for scholarly purposes may be granted by my advisor or, in his/her absence, by the Chair of the Department or the Dean of the School of Graduate Studies. It is also understood that due recognition shall be given to me and to The University of Alabama in Huntsville in any scholarly use which may be made of any material in this thesis.

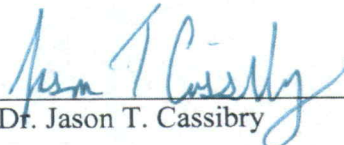

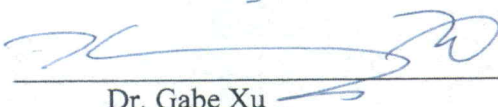
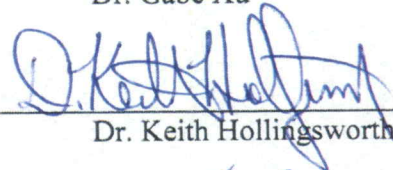
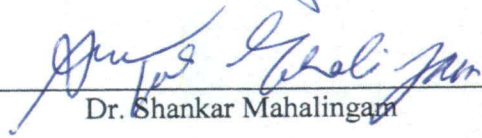
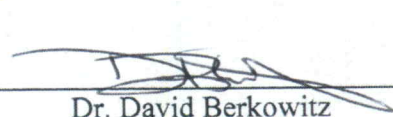
  
\_\_\_\_\_  
(Student signature)

  
\_\_\_\_\_  
(Date)

### THESIS APPROVAL FORM

Submitted by Saroj Kumar in partial fulfillment of the requirements for the degree of Master of Science in Aerospace Systems Engineering and accepted on behalf of the Faculty of the School of Graduate Studies by the thesis committee.

We, the undersigned members of the Graduate Faculty of the University of Alabama in Huntsville, certify that we have advised and/or supervised the candidate on the work described in this thesis. We further certify that we have reviewed the thesis manuscript and approve it in partial fulfillment of the requirements of the degree of Master of Science in Aerospace Systems Engineering.

 _____	8/27/18 (Date)	Committee Chair
 _____	8/24/18 (Date)	Committee Member
 _____	8/22/18 (Date)	Committee Member
 _____	9/6/18 (Date)	Department Chair
 _____	09/07/18 (Date)	College Dean
 _____	11/1/18 (Date)	Graduate Dean

**ABSTRACT**

The School of Graduate Studies  
The University of Alabama in Huntsville


Degree: Master of Science College/Department.: Engineering/Mechanical  
and Aerospace Engineering

Name of Candidate: Saroj Kumar

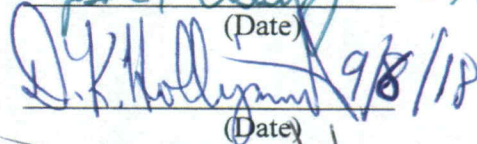
Title: Preliminary Trajectory Design Using Nuclear Fusion Propulsion for Rendezvous  
Missions to Jupiter and Saturn.

The focus of this thesis is to perform high fidelity trajectory analysis to gas giant planets Jupiter and Saturn using a nuclear fusion propulsion system for future deep space science missions. Additionally, the spacecraft has been designed with maximum Initial Mass in Low Earth Orbit (IMLEO) of 120 metric tons (mT), thus keeping it within the payload carrying capacity of NASA's SLS Block-2 Cargo launch vehicle. The propulsion system of the spacecraft utilizes the calculated propulsion parameters of fusion propulsion system. The spacecraft's trajectory has been designed in three phases namely, Earth escape and acceleration phase, coasting phase and planetary approach and orbital insertion phase. The results of the trajectory design demonstrate the key difference in terms of trip times when compared with conventional robotic missions using chemical propulsion system. The nuclear fusion propulsion system can potentially reduce trip times by a factor of three when compared with chemical propulsion systems. The high fidelity trajectory analysis also demonstrates the challenges of an orbital insertion for a finite low thrust propulsion system.

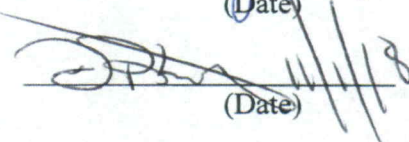
Abstract Approval: Committee Chair

  
(Date) 8/27/18

Department Chair

  
(Date) 9/8/18

Graduate Dean

  
(Date) 11/1/18



## ACKNOWLEDGEMENTS

First of all, I would like to thank my advisor and my hero *Dr. Jason Cassibry* for guiding and inspiring me throughout over the last few years. Thank you, for believing in me and giving me this opportunity to learn and work with you. Your dreams, vision and motivations have enriched my experience as a graduate student.

I would also like to acknowledge my committee members *Dr. Thomas Percy* and *Dr. Gabe Xu* for their valuable inputs and support. Many thanks to all the professors and staff of Propulsion Research Center and the department of Mechanical and Aerospace engineering for their support and encouragement.

Finally, I would like to thank my family for believing in me and supporting me throughout. Special thanks to *Sneha* for making my life complete with love and care.

## TABLE OF CONTENTS

<b>Abstract</b> .....	<b>iv</b>
<b>Acknowledgements</b> .....	<b>v</b>
<b>List Of Figures</b> .....	<b>ix</b>
<b>List Of Tables</b> .....	<b>xii</b>
<b>List Of Abbreviations And Acronyms</b> .....	<b>xiv</b>
<b>List Of Symbols</b> .....	<b>xvi</b>
<b>Chapter 1. Introduction</b> .....	<b>1</b>
<b>Chapter 2. Background Of Nuclear Fusion Propulsion</b> .....	<b>4</b>
2.1 In-Space Propulsion System.....	4
2.1.1 Chemical Propulsion.....	4
2.1.2 Non-Chemical Propulsion System.....	7
2.1.3 Advanced Propulsion System .....	8
2.1.4 Comparison of Propulsion Systems .....	9
2.2 Nuclear Fusion Propulsion System .....	10
2.3 Classification of Fusion Energy Confinement .....	11
2.3.1 Inertial Confinement Fusion .....	11
2.3.2 Magnetic Confinement Fusion.....	12
2.3.3 Magneto-Inertial Fusion.....	13
2.4 Literature review on trajectory analysis using fusion propulsion .....	14
2.4.1 Trajectory analysis from NASA Technical Publication-2003-212691..	16
.....	16
2.4.2 Trajectory analysis from NASA Technical Publication-2005-213559..	19
.....	19
2.4.3 Trajectory analysis of VISTA Spacecraft Concept.....	20
2.4.4 Discussion on Fusion Propulsion Mission Analysis.....	22
<b>Chapter 3. Systems Tool Kit Software</b> .....	<b>24</b>
3.1 Background .....	24

3.2	Orbit Dynamics .....	25
3.2.1	Spacecraft Equation of Motion .....	25
3.2.2	Orbit Propagators .....	25
3.3	STK's Astrogator Propagator .....	27
3.3.1	Astrogator Components .....	27
3.3.2	Coordinate axes.....	27
3.3.3	Models.....	28
3.3.4	Engine Models .....	30
3.3.5	B-Plane Targeting .....	31
3.4	MCS Script Setup.....	32
3.4.1	Spacecraft Configuration and Initial Elements .....	33
3.4.2	Propagate Segment.....	34
3.4.3	Maneuver Segment for Earth Escape.....	34
3.4.4	Maneuver segment for heliocentric trajectory .....	36
3.4.5	Propagate Segment.....	36
3.4.6	Maneuver segment for planetary approach.....	36
3.4.7	Propagate segment before planetary orbital insertion.....	37
3.4.8	Maneuver segment for orbital insertion.....	37
3.4.9	Maneuver segment for orbit changes and corrections .....	37
3.4.10	Propagate segment for science mission .....	37
3.4.11	Target sequence .....	38
3.4.12	Stop segment for mission conclusion .....	38
<b>Chapter 4.</b>	<b>Mission Design.....</b>	<b>39</b>
4.1	Trajectory Analysis for Planetary Escape and Capture.....	39
4.1.1	Earth Escape and Acceleration Phase .....	39
4.1.2	Coasting Phase .....	40
4.1.3	Planetary Approach and Orbital Insertion Phase .....	40
4.2	Spacecraft Design.....	41
4.3	Jupiter Rendezvous Mission .....	47
4.4	Saturn Rendezvous Mission .....	59



<b>Chapter 5. Comparison With Chemical And Field Free Fusion Propulsion</b>	
<b>Missions</b>	<b>71</b>
5.1 Juno Mission and Trajectory Design.....	71
5.1.1 Comparison with Juno Mission .....	73
5.2 Cassini-Huygens Mission and Trajectory Design.....	74
5.2.1 Comparison with Cassini-Huygens Mission.....	76
5.3 Comparison with Field-Free Fusion Propulsion Mission .....	77
<b>Chapter 6. Conclusions And Recommendations</b>	<b>78</b>
<b>Appendix A</b>	<b>80</b>
<b>Appendix B</b>	<b>86</b>
D.1 Earth's Radius of Sphere of Influence .....	86
D.2 Jupiter's Radius of Sphere of Influence .....	87
D.3 Saturn's Radius of Sphere of Influence.....	87
<b>References</b>	<b>88</b>

## LIST OF FIGURES

Figure 2.1 Chemical propulsion system using liquid propellant with a gas pressure feed system.....	5
Figure 2.2 Comparison of propulsion system based on jet power Vs $I_{sp}$ .....	9
Figure 2.3 A schematic diagram of ICF ignition point design .....	12
Figure 2.4 ITER tokamak vertical cross section.....	13
Figure 2.5 Penalty for tangentially directed thrust to planetary capture or escape..	17
Figure 2.6. 2D heliocentric trajectory from E-M L1 to Callisto roundtrip mission.	19
Figure 3.1 B-Plane geometry .....	32
Figure 3.2 Screenshot of Astrogator GUI.....	33
Figure 4.1 3D trajectory of spacecraft transfer from LEO to Earth escape .....	49
Figure 4.2 2D trajectory of spacecraft transfer from LEO to Earth escape .....	50
Figure 4.3 Spacecraft distance during Earth escape maneuver segment .....	50
Figure 4.4 Fuel used during Earth escape maneuver segment.....	51
Figure 4.5 Spacecraft C3 energy during Earth escape phase.....	51
Figure 4.6 3D trajectory of spacecraft transfer from epoch to the final HelioBurn	53
Figure 4.7 2D trajectory of spacecraft transfer from epoch to the final HelioBurn	53
Figure 4.8 Spacecraft's distance from epoch to the final burn of HelioBurn maneuver segment in Sun J2000 reference frame .....	54
Figure 4.9 Spacecraft's C3 energy from epoch to the final burn of HelioBurn maneuver.....	54
Figure 4.10 3D trajectory of spacecraft transfer from epoch to the coasting phase	55



Figure 4.11 2D trajectory of spacecraft transfer from epoch to the coasting phase	55
Figure 4.12 3D trajectory of spacecraft transfer from epoch JOI	56
Figure 4.13 2D trajectory of spacecraft transfer from epoch JOI	57
Figure 4.14 Spacecraft's captured orbit around Jupiter	57
Figure 4.15 Spacecraft's velocity during Jupiter approach phase and JOI	58
Figure 4.16 3D trajectory of spacecraft from LEO to Earth escape	60
Figure 4.17 2D trajectory of spacecraft from LEO to Earth escape	60
Figure 4.18 Spacecraft distance magnitude during Earth escape maneuver segment	61
Figure 4.19 Fuel used during Earth escape maneuver segment	61
Figure 4.20 Spacecraft's C3 energy during Earth escape maneuver	62
Figure 4.21 3D trajectory of spacecraft from LEO to the final HelioBurn	63
Figure 4.22 2D trajectory of spacecraft from LEO to the final HelioBurn	64
Figure 4.23 Spacecraft's distance from epoch to the final burn of HelioBurn maneuver segment in Sun J2000 reference frame	64
Figure 4.24 Spacecraft's C3 energy from epoch to the final burn of HelioBurn maneuver	65
Figure 4.25 3D trajectory of spacecraft from epoch to the coasting phase	66
Figure 4.26 2D trajectory of spacecraft from epoch to the coasting phase	66
Figure 4.27 3D trajectory of spacecraft from epoch to Saturn approach phase	67
Figure 4.28 2D trajectory of spacecraft from epoch to Saturn approach	68
Figure 4.29 Spacecraft's captured orbit around Saturn	68

Figure 4.30 Spacecraft's velocity during Saturn approach phase and after orbital insertion.....	69
Figure 5.1 Juno's trajectory from launch to JOI.....	73
Figure 5.2 2D trajectory of Cassini-Huygens in cruise phase from epoch to Jupiter approach.....	75
Figure 5.3 2D trajectory of Cassini-Huygens in cruise phase from epoch to Saturn orbit insertion.....	76

## LIST OF TABLES

Table 2.1 Fusion fuel reactions .....	10
Table 2.2 Trip time for direct rendezvous to outer planets .....	15
Table 2.3 Fusion propulsion spacecraft trajectory analysis results.....	18
Table 2.4 Spacecraft trajectory performance analysis .....	20
Table 2.5 Spacecraft performance for Mars roundtrip mission .....	21
Table 2.6 VISTA roundtrip mission duration from Earth to planets .....	22
Table 3.1 Central bodies' gravitational models .....	29
Table 3.2 Numerical integrator properties and step size control .....	34
Table 3.3 Calculated Sphere of Influence.....	35
Table 3.4 Control parameters to obtain desired inclination and B-plane parameters .....	38
Table 4.1 Spacecraft dry mass breakdown .....	42
Table 4.2 Spacecraft design parameters for Jupiter rendezvous mission .....	46
Table 4.3 Spacecraft design parameters for Saturn rendezvous mission.....	47
Table 4.4 Initial state orbital elements .....	48
Table 4.5 HelioBurn maneuver segment parameters.....	52
Table 4.6 Jupiter rendezvous mission timeline.....	58
Table 4.7 Initial state orbital elements .....	59
Table 4.8 HelioBurn maneuver segment parameters.....	63
Table 4.9 Saturn rendezvous mission timeline .....	70
Table 5.1 Juno spacecraft details .....	71

Table 5.2 Juno mission timeline .....	72
Table 5.3 Cassini-Huygens Spacecraft details .....	74
Table B.1 Planetary details for SoI calculation .....	86



## LIST OF ABBREVIATIONS AND ACRONYMS

2D	Two-Dimensional
3D	Three-Dimensional
AGI	Analytical Graphics Inc.
AU	Astronomical Unit
CATO	Computer Algorithm for Trajectory Optimization
CHEBYTOP	Chebyshev (Polynomial) Trajectory Optimization Program
CSC	Computer Sciences Corporation
D-D	Deuterium-Deuterium
DSM	Deep Space Maneuver
DSST	Draper Semianalytic Satellite Theory
EGA	Earth Gravity Assist
E-M L1	Earth-Moon Lagrange point 1
ESA	European Space Agency
GSFC	Goddard Space Flight Center
HPOP	High-Precision Orbit Propagator
ICF	Inertial Confinement Fusion
ICRF	International Celestial Reference Frame
IMLEO	Initial Mass in Low Earth Orbit
ISM	Interstellar Medium
ITER	International Thermonuclear Experimental Reactor
JOI	Jupiter Orbit Insertion

JPL	Jet Propulsion Laboratory
KBO	Kuiper Belt Object
LEO	Low Earth Orbit
MCF	Magnetic Confinement Fusion
MCS	Mission Control Sequence
MIF	Magneto-Inertial Fusion
MMH	Monomethylhydrazine
NASA	National Aeronautics and Space Administration
OPAG	Outer Planet Assessment Group
SESPOT	Solar Electric Geocentric Transfer with Attitude Constraints Program for Optimization of Trajectories
SEPTOP	Solar Electric Propulsion Trajectory Optimization Program
SLS	Space Launch System
SOI	Saturn Orbit Insertion
SoI	Sphere of Influence
STK	Systems Tool Kit
TCM	Trajectory Correction Maneuver
UTCg	Coordinated Universal Time in Gregorian format
VARITOP	Variational Calculus Trajectory Optimization Program
VISTA	Vehicle for Interplanetary Transport Applications
VNC	Velocity-Normal-Co-normal coordinate frame
WGS84	World Geodetic System 1984
$\Delta V$	delta V (change in velocity)

## LIST OF SYMBOLS

A	area
a	semimajor axis of ellipse
c	speed of light
C3	characteristic energy
$C_r$	coefficient of reflectivity
F	thrust
g	gram(s)
G	universal gravitational constant
$g_0$	standard gravity
$I_{sp}$	specific impulse
kg	kilogram(s)
km	kilometer(s)
$m$	mass
m	meter(s)
$\dot{m}$	mass flow rate
mT	metric ton
N	newton(s)
$P_{jet}$	jet power, W
$R, r$	magnitude distance
s	seconds
$t_r$	propulsion system run time
$t_{trip}$	total trip time

$V, v$	velocity
$V_e$	engine exhaust velocity, m/s

#### Greek Letters

$\alpha$	specific power
$\lambda$	payload mass fraction
$\mu$	gravitational parameter
$\varphi$	solar flux at 1AU
$\eta$	thrust efficiency

#### Subscripts

$e$	empty
$i$	initial
$ob$	orbiting body
$p$	propellant
$pb$	primary body
$ps$	propulsion system



## CHAPTER 1. INTRODUCTION

The objective of this thesis is to study a high fidelity mission analysis for fusion propulsion for the gas giant planets Jupiter and Saturn. Here we discuss the motivations for fusion propulsion in the context of deep space science missions, which currently take one to three decades to complete. Trip times can be reduced by a factor of three with advanced propulsion systems. However, studies in advanced propulsion systems like fusion usually make the assumption of gravity-free straight line trajectories or patched conic, and this thesis presents a more detailed study to uncover some of the technical challenges in a realistic mission trajectory.

NASA's New Horizon spacecraft took about 9.5 years from launch to reach the fly-by destination of Pluto, and a total of 14 years from its proposal[1]. The spacecraft has travelled a distance of 37.36 AU from the Sun in 11 years since its launch and is currently travelling towards a Kuiper Belt Object (KBO) '2014 MU69' for a January 2019 fly-by at a heliocentric velocity of 14.32 km/s[2]. It will further take many more years to understand the scientific data thereby taking the complete mission timeline to about a quarter of a century. The current technology with chemical or electric propulsion systems cannot provide significantly reduced trip times for robotic or human exploration to destinations like outer planets, Kuiper Belt Objects or beyond, so these mission will require about two decades to complete.

The scientific community engaged in the exploration of Outer planets and Interstellar medium (ISM) has considered many options on what could be the future

enabling technology for reducing trip times. One of the extreme examples, Voyager spacecraft crossed the termination shock in 2007, 30 years after it had been launched[3]. Some of the advanced propulsion technological breakthroughs for deep space exploration include radioisotope electric propulsion[4], [5], electric sails[6], [7], solar sail[8], [9], and beamed energy sails, matter-antimatter annihilation[10], [11].

Nuclear fusion propulsion is a promising candidate which can provide the solution for decreased travel time to the outer planets and beyond ISM[12]. Although there have been numerous studies performed on nuclear fusion spacecraft, almost all have concentrated on designing the missions for human exploration. It is expected that the first mission using fusion propulsion would be a science robotic mission which would serve as a testbed for the technology to bring down the technological risk before using it for human exploration.

Along with the development of the fusion propulsion systems it is equally important to perform the mission design and high fidelity trajectory analysis so that the capability and requirements of the propulsion system can be understood and improved. The science robotic mission needs to be designed such that the spacecraft does not require in-orbit assembly and should require only single heavy-lift launch vehicle to place the spacecraft in orbit. While there have been numerous studies on mission design using advanced propulsion concepts, most have concentrated on designing the trajectory analysis without third body effect and with very little information on spacecraft's orbital insertion maneuvers.

This thesis describes the spacecraft design and trajectory analysis for a fusion propulsion spacecraft. The mission design consists of rendezvous mission to Jupiter and

Saturn. The rendezvous mission has been specifically designed so that the trip time is minimized. The trajectory of the fusion propulsion spacecraft for a rendezvous consist of three phases. The first phase consist of acceleration phase. During this phase the spacecraft accelerates from the parking LEO orbit towards the destination planet using thrust provided by the fusion propulsion system. The second phase consist of coasting phase. During this phase the spacecraft is in hibernation mode and its propulsion system is off. This phase would only require Trajectory Correction Maneuvers (TCM) to make sure that the spacecraft is pointed at the right direction. The final third phase is planetary approach phase and orbit insertion phase. During this phase the spacecraft would reduce its velocity with respect to the destination planet and align itself for the required orbit around the destination planet. AGI's STK Astrogator tool[13] has been used to design fusion propulsion engine for finite maneuvers and high-fidelity orbit propagation.

The following thesis consists of the above mentioned mission design in detail where Chapter 2 consists of a brief description of fusion propulsion systems and various trajectory analyses conducted previously. Chapter 3 consists of detailed description of the STK Astrogator for trajectory analysis using a fusion propulsion system. Chapter 4 explains the strategy for spacecraft design and trajectory analysis for Jupiter and Saturn. Chapter 5 compares the trajectory of a fusion propulsion spacecraft and conventional spacecraft using chemical propulsion such as with Juno and Cassini-Huygens missions. Finally, concluding remarks and future considerations are provided in chapter 6.



## CHAPTER 2. BACKGROUND OF NUCLEAR FUSION PROPULSION

The propulsion system of a spacecraft is used to provide forces or torques in outer space to maneuver the spacecraft. These maneuvers propel the spacecraft for orbit changes, station keeping and attitude adjustment. The following chapter includes the classification of in-space propulsion systems with discussion on nuclear fusion propulsion system. A literature review on trajectory analysis with fusion propulsion systems is given and limitations of the previous work reported in the literature is given. This review motivated the work presented in this thesis.

In the subsequent discussion frequent use of thrust, specific impulse and jet power are made to draw comparison among propulsion systems. The ideal rocket equation is a solution to determine the performance of any rocket and is given by[14],

$$\Delta V = I_{sp} g_o \ln \left( \frac{m_i}{m_f} \right) \quad (2.1)$$

where,  $\Delta V$  is the change in velocity (m/s),  $I_{sp}$  is the specific impulse (s),  $g_o$  is the standard gravity (9.81 m/s),  $m_i$  is the initial mass and  $m_f$  is the final mass of the rocket.

### 2.1 In-Space Propulsion System

The most common in-space propulsion system are classified into three types, namely Chemical, Non-chemical and Advanced Propulsion systems[15].

#### 2.1.1 Chemical Propulsion

The most common source of energy to generate thrust for orbit maneuver or attitude correction for a spacecraft in space has been using chemical combustion. Barring few deep space mission using electric propulsion, almost all interplanetary science missions have

used onboard chemical propulsion for orbit maneuvering. Most of the spacecraft's onboard propulsion system use a fuel and oxidant. The chemical reaction between fuel and oxidizer releases energy, which results in gaseous products. The gaseous products are then expelled through a rocket nozzle which then generates thrust for the spacecraft. The chemical propulsion system can be classified into four types based on the physical state of the propellant.

Chemical propulsion systems have the capacity to provide thrust to weight ratios of up to 200:1 by using chemical reactions to heat and expand large amount of propellant from conventional converging-diverging nozzle engines[16]. This propulsion system have low specific impulse (194-468 seconds) compared to other propulsion systems thus decreasing the efficiency of the engine drastically. Typical propellants used for chemical propulsion are monopropellants, bipropellants or liquid cryogenics. Figure 2.1 shows the pressure-fed liquid propellant chemical propulsion system.

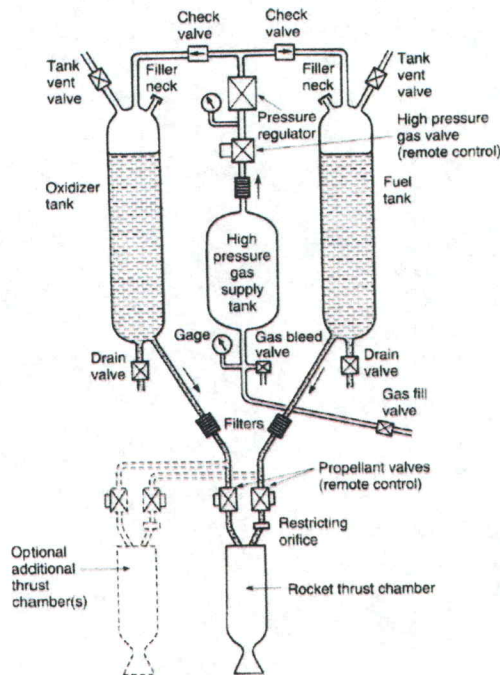


Figure 2.1 Chemical propulsion system using liquid propellant with a gas pressure feed system[16].

### **2.1.1.1 Solid Propellant Systems**

In the solid propellant systems, the propellant is stored in a combustion chamber which is usually in a shape of cylinder with hollow central core. The shape of the central core is used to define the burning rate of the propellant. The resulting hot gases upon the burning of propellant flows through the rocket nozzle to impart thrust on the spacecraft. The propellant burning rate and solid propellant charge configuration mainly define the propulsion system performance. The biggest advantage of this propulsion system is the simplicity in design which does not have any moving parts and is not as complex when compared to liquid propulsion systems. This system is normally used as a final boost stage of the spacecraft after it has been released from the launcher. However, some of the disadvantages of this propulsion system include low specific impulse and inability to be throttled during operation.

### **2.1.1.2 Liquid Propellant Systems**

The liquid propellant system can further be classified into three categories as cryogenic, monopropellant and bipropellant systems. The cryogenic propulsion system uses cryogenic fuel and oxidizer that are gases liquefied. These propulsion systems are normally not used for deep space due to their requirement of specific temperatures and pressure at operation. The common fuel used is liquid hydrogen and liquid oxygen as oxidizer. The monopropellant propulsion system uses a single propellant that contains both fuel and oxidizer. This type of propellants are most suited for deep space missions due to their storability for long duration of time. Some of the most common monopropellants are hydrazine and hydrogen peroxide. The bipropellant propulsion system consists of separate fuel and oxidizer. The performance parameters of this propulsion system is greater than the



monopropellant propulsion system. Some of the most common bipropellants used are kerosene and monomethylhydrazine (MMH) as fuel and liquid oxygen and nitrogen tetroxide ( $N_2O_4$ ) as oxidizer.

### **2.1.1.3 Gaseous Propellant Systems**

The gaseous propellant system or cold gas propulsion system is usually used for attitude control and low thrust maneuver of a spacecraft. This propulsion system uses high pressure gas such as nitrogen and helium. Due to their very low thrust generation capacity and relatively heavy tank requirements they are not suited for deep space missions.

### **2.1.1.4 Hybrid Propellant Systems**

The hybrid propellant systems consist of propellants in two different phases – Solid and liquid. Generally, the fuel used is in solid phase and the oxidizer in liquid phase because the solid oxidizers are low performing and performance of solid fuel can be improved using fuel additives. The hybrid propulsion system are more suited due to their simpler design when compared to liquid propulsion system and have the capability to be throttled or restart during the mission in real time.

### **2.1.2 Non-Chemical Propulsion System**

Non-Chemical propulsion systems perform similar tasks as chemical propulsion but without chemical reactants. These propulsion systems use electrostatic, electromagnetic, fission reactions or energy supplied from external sources to generate thrust for the spacecraft. Non-Chemical propulsion systems are much more efficient when compared with chemical propulsion due to their ability to have higher specific impulse or in some cases requiring no propellant at all. Although the specific impulse is very high the

thrust produced is moderate or sometimes negligible when compared to chemical propulsion. Electric propulsion[17], nuclear thermal propulsion[18], solar sail propulsion[19] and tether propulsion[20] are some of the examples of non-chemical propulsion systems.

### **2.1.3 Advanced Propulsion System**

The advanced propulsion systems are those that use either the chemical or non-chemical physics to generate thrust for the spacecraft. The departures from the previously mentioned systems are explained below. These propulsion systems are usually classified with technology readiness levels[21] of less than three thus, are yet to be declared matured but show promising results based on theoretical analysis. The advanced propulsion systems have capacity to produce low to moderate thrust with very high specific impulse. Some examples of advanced propulsion systems include fusion propulsion, antimatter propulsion and beamed energy propulsion[22][23]. Among the mentioned advanced propulsion systems, this treatise will study the capabilities of fusion propulsion system for deep space exploration. Motivations for choosing fusion propulsion can be found in Cassibry et al [12]. The primary arguments for fusion include the following. First, energy storage for fusion and fission fuels are  $10^6$  times higher on an energy per unit mass basis compared with chemical reactions. Second, the energy release can lead to high specific impulse (10,000 to  $10^6$  s) and moderate thrust (100 to 10,000 N) enabling mission trip times of 1/3 or better compared with chemical missions. Finally, fusion and fission/fusion hybrid systems can operate anywhere in space, compared to many other systems that rely on proximity to the Sun (0.1 to 5 AU) for the energy source.

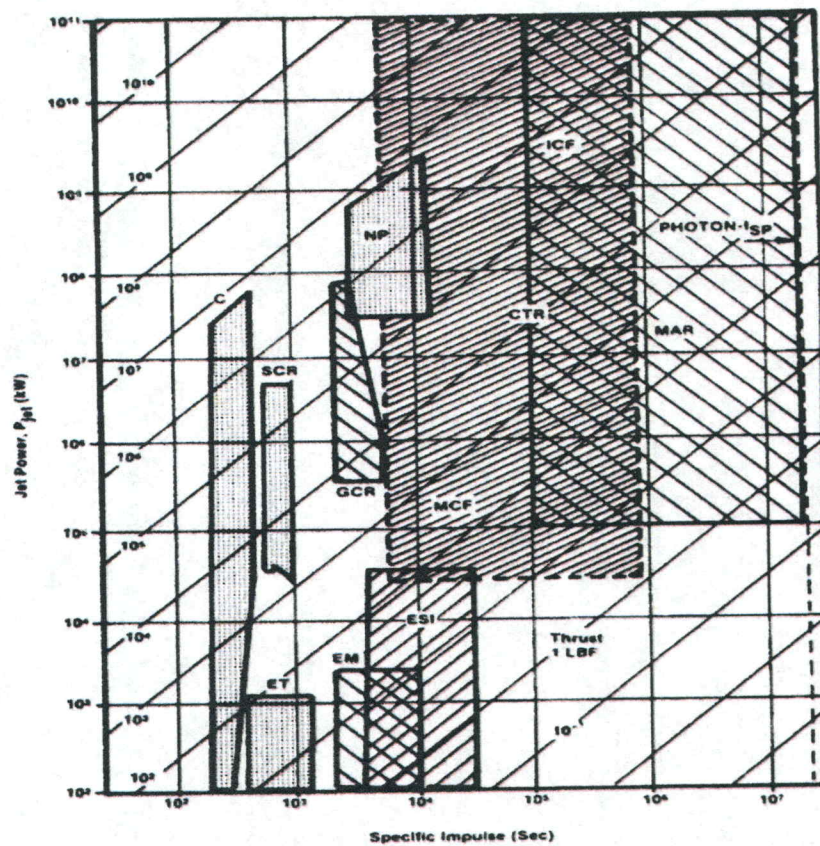


### 2.1.4 Comparison of Propulsion Systems

One of the important parameter to measure the propulsive capability is jet power which is given by,

$$P_{jet} = \frac{1}{2} \dot{m} V_e^2 \quad (2.1)$$

The jet power vs specific impulse for the propulsion system in Figure 2.2 reveals the merits of chemical, electrical, fusion and other propulsion systems.



- |                                         |                                  |
|-----------------------------------------|----------------------------------|
| chemical C,                             | electromagnetic EM,              |
| electrothermal ET,                      | electrostatic ion thruster ESI,  |
| solid core reactor SCR,                 | gas core reactor GCR,            |
| nuclear pulsed (orion type) NP,         | magnetic confinement fusion MCF, |
| controlled thermonuclear reactions CTR, | mass annihilation rocket, MAR.,  |
| inertial confinement fusion ICF,        |                                  |

Figure 2.2 Comparison of propulsion system based on jet power Vs  $I_{sp}$ [24].

It can be noted that the chemical propulsion system can produce large amount of jet power but have limited range of specific impulse of about 194-468 seconds. Thus, chemical propulsion system can generate large thrust at an expense of large amount of propellants which decreases the payload mass fraction of the spacecraft considerably. The electric propulsion system have larger specific impulse but at an expense of reduced jet power and thrust. However, the fusion propulsion system demonstrates the capability of very high specific impulse and moderate thrust levels. Therefore, with these propulsion parameters fusion propulsion has shown the potential to reduce the trip times for deep space missions by a factor of three when compared with chemical propulsion systems.

## 2.2 Nuclear Fusion Propulsion System

Nuclear fusion occurs when light atomic nuclei overcome the mutual coulomb repulsion via sufficient kinetic energy and quantum tunneling and combine, thereby forming a heavier atomic nuclei. Table 2.1 lists some of the more promising fusion reactions, enabled by higher cross sections compared with other minor side reactions.

Table 2.1 Fusion fuel reactions[25]

Fusion Fuel	Chemical reaction	Energy released (MeV)
Deuterium-Deuterium	${}^2_1D + {}^2_1D \rightarrow {}^2_1T + p^+$	4.03
	${}^2_1D + {}^2_1D \rightarrow {}^3_2He + n^0$	3.27
Deuterium-Tritium	${}^2_1D + {}^3_1T \rightarrow {}^4_2He + n^0$	17.59
Deuterium- Helium-3	${}^2_1D + {}^3_2T \rightarrow {}^4_1He + p^+$	18.35
Proton-Boron-11	$p^+ + {}^{11}_5B \rightarrow 3{}^4_2He$	8.7

The fusion reaction rate,  $r$ , between two species with number densities  $n_1$  and  $n_2$  is given by,

$$r = \frac{n_1 n_2}{1 + \delta_{12}} \langle \sigma v \rangle_{12} \vartheta \quad (2.2)$$

where  $\langle \sigma v \rangle$  is the average of the cross section ' $\sigma$ ' over the relative velocities ' $v$ ',  $\delta_{12}$  is the Kronecker delta function, and  $\vartheta$  is the volume of reacting plasma.

The energy released per unit mass of fuel is  $\sim 10^{14}$  J/kg, which is one million times more energy per unit mass compared with chemical reactions. Among mentioned fusion reactions possible, reaction between deuterium (D) and tritium (T) is considered to be one of the most feasible. Deuterium can be extracted in large amount from ocean's sea water and tritium can be produced by breeding in a traditional nuclear fission reactor.

### 2.3 Classification of Fusion Energy Confinement

Fusion energy is classified based on the specific confinement method used to hold together the burning plasma. Inertial Confinement fusion[25] and Magnetic Confinement fusion[26] are the main approaches for the fusion confinement. A few other types of confinement methods are Inertial electrostatic confinement[27] and Magneto-Inertial fusion[28].

#### 2.3.1 Inertial Confinement Fusion

Inertial Confinement Fusion (ICF) reactions depend on the mass inertia. A small volume of fusion fuel in the form of pellet is used to heat the fuel rapidly. Typically, lasers are used to compress and heat the fuel to initiate thermonuclear ignition[25]. A schematic of ICF system is shown in Figure 2.3. Lawrence Livermore National Laboratory studied a conceptual design in space propulsion called Vehicle for Interplanetary Transport



Applications (VISTA) powered by advanced ICF technology. The conceptual VISTA spacecraft theoretically had a capacity to deliver 100 mT of payload and a total roundtrip time to Mars in 145 days[29].

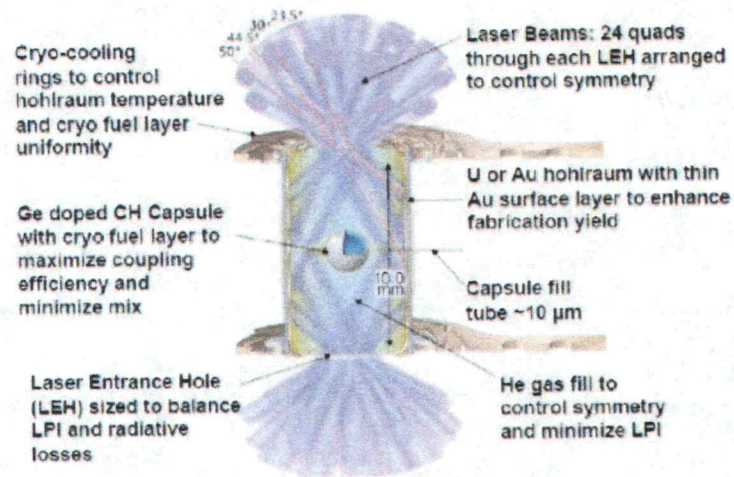


Figure 2.3 A schematic diagram of ICF ignition point design[30].

### 2.3.2 Magnetic Confinement Fusion

Magnetic Confinement Fusion uses a magnetic field in which the magnetic pressure exceeds the static pressure of the confined plasma. Two of the most commonly studied configurations for MCF are stellarators and tokamaks. Unfortunately, this technology has shown less prospect of a future propulsion system due to heavy mass of these confinement configurations. These confinement methods have potential to be used for terrestrial power generation. The International Thermonuclear Experimental Reactor (ITER) is currently working on the development of world's largest magnetic confinement plasma physics experiment. Once operational, it will have a capacity to produce 500 megawatts of thermal output power with consumption of 50 megawatts into tokamak thus resulting in a gain of about 10[31].

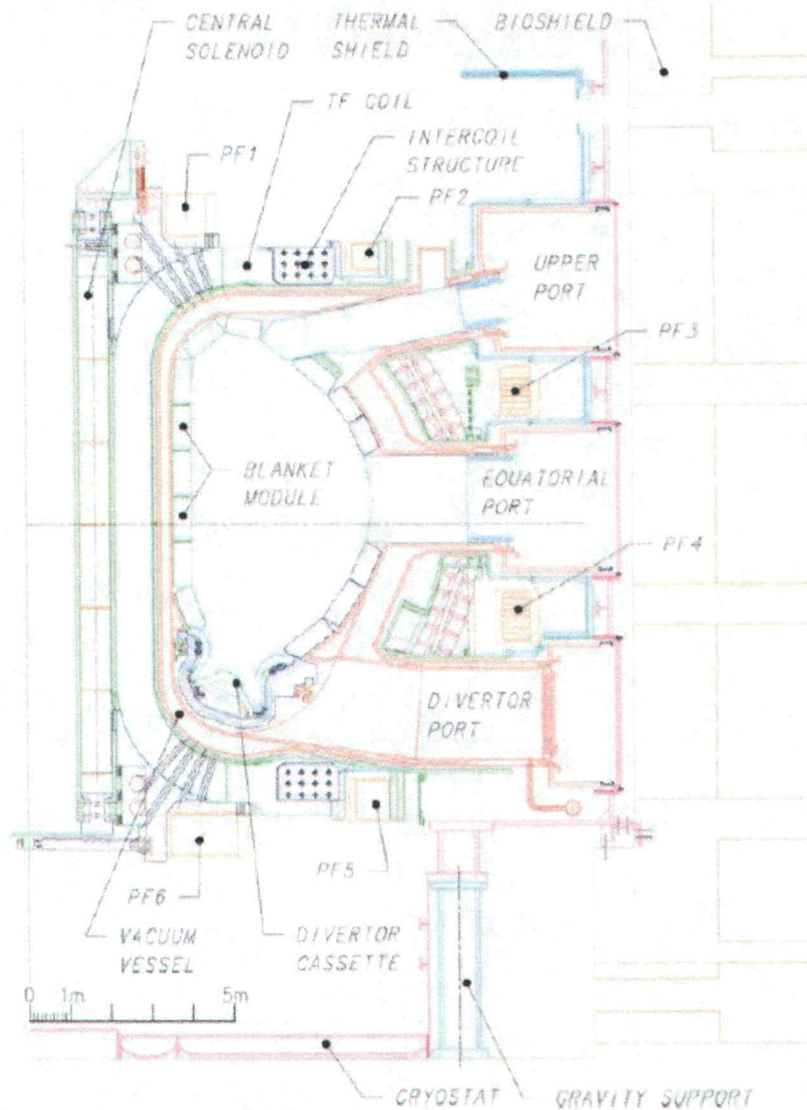


Figure 2.4 ITER tokamak vertical cross section[31].

### 2.3.3 Magneto-Inertial Fusion

Magneto-Inertial Fusion uses the concept of inertial confinement fusion for compressional heating and magnetic confinement fusion for enhanced alpha heating. The use of magnetic confinement helps in reducing the required implosion velocity and also decreases the thermal conductivity[32]. The areal density requirement for the fusion reaction also reduces considerably which makes the ignition of fusion reaction possible at a low density ( $0.01 \text{ g/cm}^2$ )[33]. Based on the use of liner system there are many subsets of

MIF such as magnetized target fusion, z-pinch and theta pinch. Reference [34] further provides the detailed description of fusion propulsion classification that includes explanation on gasdynamic mirror for magnetic confinement and fusion-fission hybrid system.

## **2.4 Literature review on trajectory analysis using fusion propulsion**

Early trajectory analysis for a spacecraft propelled with a fusion propulsion system is necessary to evaluate the performance. Fusion is still at a low technology readiness level, and such analysis, is shown to enable new mission capability, and motivates further development. Fusion propulsion, a very high specific impulse and moderate thrust system, can enable a completely new class of space missions which would never be possible with any propulsion system available today.

Trajectory analysis for interplanetary missions with chemical propulsion system were conducted immediately after the first satellites were launched into space[35]. The trajectory analysis for a chemical propulsion spacecraft were initially performed with patched conic approximation where only two bodies are considered at one time to solve the two-body equations within the boundary conditions[36]. The  $\Delta V$  required for the mission using chemical propulsion is calculated using impulsive method because a chemical engine generates high thrust and burns for a very small duration compared to the total trip time. Rendezvous trip times in these initial studies are summarized in the table 2.2 below.



Table 2.2 Trip time for direct rendezvous to outer planets

Mission	Minimum launch energy, $C_3$ (km <sup>2</sup> /sec <sup>2</sup> )	Rendezvous trip time (Years)
Earth-Jupiter	86.5	2.5
Earth-Saturn	108.8	6.1
Earth-Uranus	126.1	16.0
Earth-Neptune	135.0	30.7
Earth-Pluto	135.3	45.7

Unlike Chemical propulsion impulsive burns, the burn time for a fusion propulsion is much longer. Due to the small thrust generated by the fusion propulsion, the forces and perturbations from the multiple celestial bodies can have higher impact on the trajectory compared to a high thrust system. This problem can be solved by the use of finite burn analysis using high fidelity trajectory analysis.

The trajectory design using advanced propulsion system with low thrust system is challenging due to various reasons. The spacecraft burns propellant for a significantly longer duration during the trip time, and the control variables for the trajectory analysis needs to be continuously optimized[37]. Various software tools are available for low thrust specific missions to design trajectory analysis. Some of the representative tools are CHEBYTOP, SEPSOT, VARITOP, SEPTOP[38] and Systems Tool Kit[13]. VARITOP was one of the earliest optimization program developed by NASA and has been used for many preliminary mission studies by NASA centers. VARITOP sister program, SEPTOP, along with Computer Algorithm for Trajectory Optimization (CATO) was used to provide accurate trajectory model for Deep Space 1 mission[39]. While rigorous mission analysis is merited, as summarized below, such analysis has been limited for fusion propulsion.

Frequently, major assumptions are made using straight line trajectory and gravity free models. Below a summary of the mission analysis results are provided for some of the more prominent fusion propulsion studies.

#### **2.4.1 Trajectory analysis from NASA Technical Publication-2003-212691**

The NASA Technical Publication 2003-212691 investigated crewed missions to Callisto using five various propulsion concepts[40]. The first three mission concepts used magnetized target fusion with fuel as either deuterium-deuterium or deuterium-helium-3. The fourth and fifth option included propulsion system using a magnetoplasmadynamic thruster assembly. A stay time of 180 days on Callisto was required due to the need of alignment of Jupiter and Earth in order to reduce the total  $\Delta V$  requirement. The study also performed a trajectory analysis with 30 day stay on Callisto in order to demonstrate the capability of the fusion propulsion system. The total trip time excluding Earth escape and capture was constrained to 650 days due to the reduced mission  $\Delta V$  requirement.

The departure and return position of the spacecraft was considered from Earth-Moon Lagrange 1 point. Most of the trajectory analysis for the study was concentrated towards heliocentric phase of the trajectory. Two body Sun centered VARITOP trajectory tool was used to model the heliocentric trajectory of the mission. The planets are assumed to be without mass and the targeting constraints for the spacecraft was to match the position and velocity of the spacecraft with respect to the destination planet. The planetary departure and capture  $\Delta V$  were approximated using Figure 2.5 from reference[41].



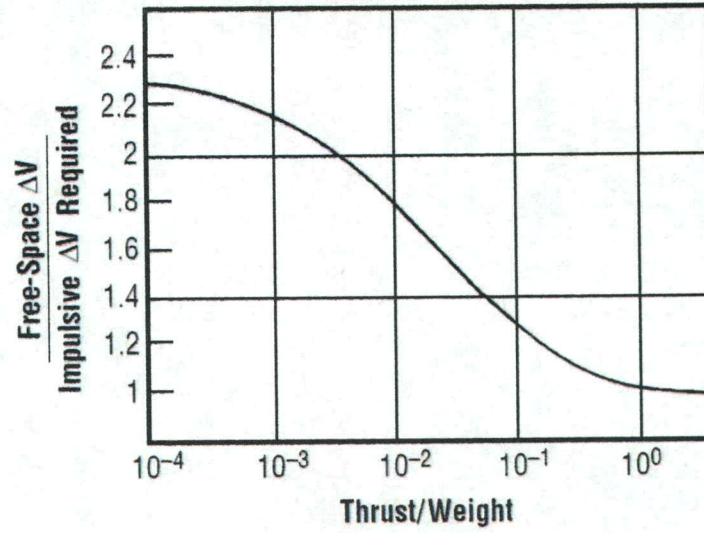
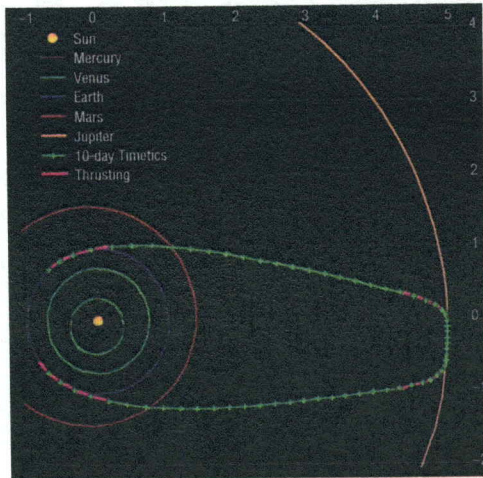


Figure 2.5 Penalty for tangentially directed thrust to planetary capture or escape[41].

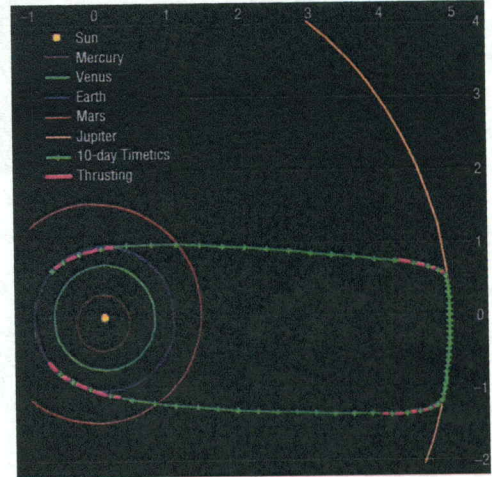
The results of the trajectory analysis of fusion propulsion spacecraft for D-D 30 day stay, D-D 180 days stay and D-He-3 180 day stay are given in table 2.3. Figure 2.6 shows the 2D heliocentric trajectory of D-D 30 days stay, D-D 180 days stay and D-He-3 180 days stay time missions.

Table 2.3 Fusion propulsion spacecraft trajectory analysis results [36]

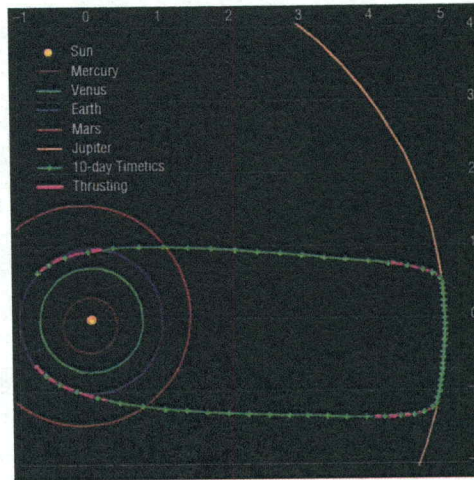
Propellant	Deuterium-Deuterium	Deuterium-Deuterium	Deuterium-Helium-3
Total mission duration	654 days	652 days	652 days
Departure (E-M L1)	22 Apr 2045	26 Apr 2045	27 Apr 2045
Flight to Callisto	331 days	249 days	249 days
Time in Callisto orbit	33 days	183 days	183 days
Total thrust time	258 days	212 days	215 days
Specific impulse	70,400 s	70,400 s	77,000 s
Jet power	1.072 GW	2.038 GW	2.017 GW
Initial mass	645,173 kg	756,162 kg	691,892 kg
Payload mass	163,933 kg	163,933 kg	163,933 kg
Propulsion system mass	116,021 kg	121,333 kg	118,400 kg
Propellant mass	106,000 kg	165,000 kg	142,000 kg



(a) *D-D 30 days stay mission*



(b) *D-D 180 days stay mission*



(c) *D-He-3 180 days stay mission*

Figure 2.6. 2D heliocentric trajectory from E-M L1 to Callisto roundtrip mission.

### 2.4.2 Trajectory analysis from NASA Technical Publication-2005-213559

The NASA Technical Publication 2005-213559 proposes the conceptual spacecraft design using spherical torus nuclear fusion reaction for rendezvous mission to Jupiter and Saturn[42]. The designed spacecraft has IMLEO of 1,690 mT with 172 mT of payload including possible weight growth contingency.  $D_2$  and  $^3He$  were selected as fuel for fusion propulsion system due to their possible abundance in destination planet's atmosphere.



The departure and arrival position of the spacecraft was considered at planetary escape orbit (C3~0) with maximum duration of the mission constrained to be 12 months. For trajectory analysis, an analytic closed form solution using high specific impulse/ high thrust algorithm[43] in a field-free space was implemented to determine the approximate duration of the trip time and spacecraft performance analysis. Table 2.4 shows the overall trajectory performance of the spacecraft to Jupiter and Saturn missions.

Table 2.4 Spacecraft trajectory performance analysis[44]

Destination mission type	Jupiter rendezvous	Saturn rendezvous
Propellant	Deuterium-Helium-3	Deuterium-Deuterium
Departure/ arrival orbit	C3~0	C3~0
Total trip time	118 days	212 days
Travel distance	4.70 AU	9.57 AU
IMLEO	1690 mT	1699 mT
Payload mass	172 mT	172 mT
Specific impulse	35,435 s	47,205 s

### 2.4.3 Trajectory analysis of VISTA Spacecraft Concept

A Vehicle for Interplanetary Space Transport Application Powered by Inertial Confinement Fusion (VISTA) is the conical shaped spacecraft concept developed for the human exploration of Mars and beyond[45]. The initial design considers deuterium and tritium as fuel capsules which is surrounded by added hydrogen mass (called as expellant). The ICF based engine is estimated to have power/mass ratio of 20W/g at the repetition rate of 30Hz, thus having a capability of about 20,000 s of specific impulse.

The spacecraft is designed in order to have payload capacity of 100 tons with initial mass varying for each mission. Due to the massive size of the spacecraft, in-orbit assembly will be required in LEO at an altitude of 700 km. For trajectory analysis, a NASTRAN computer code at JPL and analytic trajectory code IFRTRIP was used to determine approximate trip times. The flight time for a roundtrip mission to Mars was calculated to be 145 days with total initial wet mass of 6000 mT. Similarly, a roundtrip mission to Titan could be performed in 500 days with 100 ton payload and total initial mass of 2500 tons (including 1400 tons of propellant). Table 2.5 shows the spacecraft performance for Mars roundtrip mission and table 2.6 shows the capability of VISTA spacecraft for a round trip mission from Earth to the planets with target gain of 1500.

Table 2.5 Spacecraft performance for Mars roundtrip mission

Total trip time	145 days
Propellant	D-T
Departure orbit	700 km circular
Mass flow rate	1.54 kg/s
Specific impulse	27,200 s
Jet Power	17.80 GW
IMLEO	6000 mT

Table 2.6 VISTA roundtrip mission duration from Earth to planets

Mercury	160 days
Venus	108 days
Mars	145 days
Jupiter	422 days
Saturn	735 days
Uranus	1425 days
Neptune	2134 days

There have been further several studies conducted on a fusion powered spacecraft for interplanetary and interstellar missions using the concept of pulsed fusion, pulsed fission-fusion and Z-pinch based nuclear propulsion system mentioned in Ref.[39]–[43].

#### 2.4.4 Discussion on Fusion Propulsion Mission Analysis

Although there have been many studies conducted on the mission design of fusion powered spacecraft, almost all have concentrated on spacecraft subsystem design, assembly characteristics and fusion engine development with little emphasis on a detailed end-to-end trajectory analysis. Most of the trajectory analysis has been concentrated towards the heliocentric trajectory of the mission. It is equally important to understand how a fusion powered spacecraft can obtain the required  $\Delta V$  to depart from Earth's Sphere of Influence (SoI), use TCM's during it heliocentric orbit and finally align itself to achieve the required orbit at the destination planet. Even though almost all the studies on mission design have concentrated towards a human piloted mission, the author believes that the first mission using fusion propulsion will be a robotic mission. The robotic mission would



require a smaller propulsion system compared to a human piloted vehicle, potentially launched and deployed from a single heavy lift rocket. Further, initial robotic missions will buy down the technology risk and increase confidence that the new fusion propulsion systems are reliable and safe for deep space human missions. The work presented in the thesis concentrated on the spacecraft and trajectory analysis for a robotic rendezvous mission to Jupiter and Saturn with complete details from spacecraft's launch to its orbit insertion at the destination planet.

The author hopes that the work presented in the thesis will further narrow down the margins of various parameters currently assumed for the spacecraft design such as specific power, IMLEO and fuel utilization etc. The mission design presented does not show the final design but only helps in further improvement of the major spacecraft subsystem design and trajectory analysis.

## CHAPTER 3. SYSTEMS TOOL KIT SOFTWARE

Systems Tool Kit (STK) is a physics based commercial off-the-shelf software package developed by Analytical Graphics, Inc. (AGI) for evaluating the performance of complex models for land, sea, air or space based systems[13]. Under the AGI's Educational Alliance Program (EAP), the STK licenses are free for academic research. The software requires Windows operating system (Windows 10, 8, 7, windows server 2012). STK's Astrogator analysis module was used to perform mission design and trajectory analysis for the work presented in the thesis in Chapter 4 and 5.

### 3.1 Background

The Systems Tool Kit formerly known as Satellite Tool Kit was initially developed by NASA's Goddard Space Flight Center (GSFC) in 1989 to be able to run on personal computers rather than on mainframe computers. The initial program was developed by Computer Sciences Corporation (CSC) which was known as 'Swingby' mainly because the first mission it was tasked to support was the double lunar swingby 'Wind' mission[51]. Later, NASA's GSFC Flight Dynamics Facility collaborated with Naval Research Laboratory to further enhance the capabilities of 'Swingby' which could support lunar and asteroid rendezvous missions. In 1994, the commercial version of the software was known as Navigator which was again enhanced in 1996 and renamed as STK/Astrogator.

STK/Astrogator has been used for many conceptual mission design and trajectory analysis studies like rendezvous in lunar distant retrograde orbit[52], Sun-Mars liberation point[53] and low energy interplanetary transfers[54]. The software has also been used for operations on many missions such as NASA's Lunar Atmosphere and Dust Environment

Explorer (LADEE)[55], Solar and Heliospheric Observatory (SOHO)[56], Advanced Composition Explorer (ACE)[57] and AsiaSat 3 rescue missions[51].

## 3.2 Orbit Dynamics

### 3.2.1 Spacecraft Equation of Motion

The spacecraft's equation of motion in orbit can be determined using Newton's laws of motion. We know Newton's second law as,

$$\frac{d(mv)}{dt} = \sum F_{ext} \quad (3.1)$$

where,  $m$  is the total mass of the spacecraft,  $v$  is the spacecraft's velocity,  $t$  is time and  $F_{ext}$  is total external forces. Solving the above equation for two body problem with perturbations gives,

$$\frac{d^2r}{dt^2} = -\frac{\mu}{r^3}\vec{r} + f_p \quad (3.2)$$

where,  $\mu$  is called as gravitational parameter and  $f_p$  is the sum of all perturbing acceleration including central body direct nonspherical perturbation, direct third body point mass perturbation, indirect third body point mass perturbation, spacecraft thrust atmospheric drag and solar radiation pressure perturbation.

### 3.2.2 Orbit Propagators

The orbit propagators are used to determine the motion of the spacecraft over a period of time. With the implementation of Newton's laws, the trajectory of the spacecraft can be determined based its initial state and the perturbing forces acting on the spacecraft. There are three different types of orbit propagation techniques namely, numerical integration[58], analytical[59] and semianalytical[60]–[62].



The analytical propagation method approximates the spacecraft's ephemeris using only the initial state of the spacecraft and time. The central body for the spacecraft is always considered as a point mass. Some of the models include the J2 perturbations (effect of asymmetry in Earth's gravitational field) and J4 perturbations (effect of Earth's oblateness) and simple atmospheric drag model. These propagators are also known as low fidelity propagators due to inaccuracies when the model propagates for a longer period of time. These are best used to determine a spacecraft's trajectory around Earth to track and communicate without having to maneuver the spacecraft.

The semianalytical propagation method provides more accuracy than the analytical propagation technique. It uses numerical methods with less approximations to determine the spacecraft's trajectory. These propagators are also known as medium fidelity propagators. Draper Semianalytic Satellite Theory (DSST) orbit propagator can be categorized under semianalytical propagators which is used for maneuver planning of spacecraft in Earth's Orbit and maintain the space object catalog[63], [64]. The semianalytical propagators available in STK are Long term Orbit Predictor (LOP) and SGP4 for non-LEO satellites.

The Numerical propagators are the most accurate when compared with analytical and semianalytical propagation techniques. Thus, they are also known as High fidelity orbit propagators. These propagators typically use all the forces acting on spacecraft to determine the realistic trajectory. Numerical propagators are used for spacecraft operations and studies which involve high accuracy analysis. STK has two high fidelity numerical propagators namely Astrogator and High precision Orbit Propagator (HPOP). The trajectory analysis presented in the thesis uses STK Astrogator propagator.

### **3.3 STK's Astrogator Propagator**

STK's Astrogator propagator analysis module is intended to design and analyze spacecraft trajectories and orbital maneuvers. The Astrogator propagator module executes the Mission Control Sequence (MCS) designed by the user and simultaneously calculates the spacecraft's ephemeris. The capabilities of Astrogator include the high-fidelity orbit propagation and modeling impulsive and finite maneuvers of spacecraft. Various algorithms and models used in Astrogator include numerical integration using cowell's formulation, variation of parameters for orbit propagation, gravitational and atmospheric models for many planets. The user can define the targeting methods including differential corrector which allows the user to determine the values of control parameters to satisfy the desired results. The user interface and mission control sequence segments available in Astrogator analysis module are described in detail in Appendix A.

#### **3.3.1 Astrogator Components**

The Astrogator components allows the user to define and create specific components required for mission design analysis. Components can be used using single component select window which cannot be edited. The multi component select window can be used as per the mission requirement by editing the elements of the components. Some of the components used for analysis in this thesis are central bodies, constraints, engine models, propagator function, propagators, stopping conditions and thruster sets etc.

#### **3.3.2 Coordinate axes**

To define the initial orbital elements of the spacecraft with respect to its central body, Earth J2000 coordinate system was used. Other coordinate systems such as International Celestial Reference Frame (ICRF) and J2000 Ecliptic were used to extract



output data. During orbit insertion, target body's centered reference frame was used. STK provides many coordinate systems for central bodies under vector geometry tool. Some of the commonly used reference frame are ICRF, J2000, J2000 ecliptic defined by FK5 IAU76 theory, Mean of Epoch J2000, True Equator True Equinox axes for sun system only.

### 3.3.3 Models

Various gravitational and atmospheric models are available in STK to determine the precise forces acting on the spacecraft. The main forces acting on the spacecraft are central body gravity, solar radiation pressure, third body gravitational force and atmospheric drag and forces due to oblateness of a spacecraft's parent celestial body.

#### 3.3.3.1 Gravitational Model

Newton's law of universal gravitation between two objects can be described as,

$$F = G \frac{m_1 m_2}{r^2} \hat{r} \quad (3.3)$$

where,  $m_1$  and  $m_2$  are the masses of primary and secondary bodies,  $r$  is the distance between them,  $F$  is the force on  $m_2$  due to  $m_1$  and  $G$  is the universal gravitation constant which has a value of  $6.674 \times 10^{-11} \text{ Nm}^2\text{kg}^{-2}$ . Due to direct and indirect third body point mass perturbation and central body direct non-spherical perturbation accurate gravitational models of celestial bodies are required for orbit prediction.

Most of the central bodies in STK have specific gravitational models available to select from. The user can define the gravitational model by specifying gravitational parameter in the  $\text{km}^3/\text{sec}^2$ , the celestial body's reference distance from the center of mass to its surface, J2- first order oblateness effects, J3- first order longitudinal variations and



J4- second order oblateness of the celestial body. Some of the models available in STK for non-editable central bodies include are mentioned in table 3.1

Table 3.1 Central bodies' gravitational models

Central Body	Model	Description
Earth	WGS84	The World Geodetic System 1984 (WGS84) in Earth fixed reference frame gives the detailed gravitational model of Earth by defining shape of the Earth, its mass, angular velocity[65].
Moon	LP150Q	The lunar gravity model is developed using the data from Lunar Prospector mission[66].
Mars	GMM2B	The Mars gravitational field model is developed using the data from Mars Global Surveyor[67].
Jupiter	JUP230	Jupiter gravitational model is determined numerically using the astrometric observations and data from the previous spacecraft's[68]
Saturn	Astron2004	Saturn gravitational model is determined numerically using the astrometric observations and data from the Pioneer 11, Voyager and Cassini spacecraft[69].
Uranus	Ura083Spice	Uranus gravitational models is derived from the SPICE gravity coefficients, Earth based astrometry and Voyager 2 spacecraft data[70].
Neptune	AstronAstro1991	Neptune gravitational model is derived from Earth based observations and data provided from previous spacecraft's[71].

### 3.3.3.2 Solar Radiation Pressure Model

The spacecraft's cross section is assumed perpendicular to the direction of solar radiation by default. The user can change the orientation of the spacecraft as per the trajectory. User also needs to mention the reflectivity of the spacecraft, where a fully reflective spacecraft body has coefficient of 2.0 and non-reflective body has coefficient of 1.0. The acceleration due to solar radiation pressure is given by

$$\vec{a} = -C_r \frac{A K \phi}{M c} \left( \frac{1}{R_{AU}} \right)^2 \hat{r}_s \quad (3.4)$$

where,  $C_r$  is coefficient of reflectivity,  $A$  is area of spacecraft,  $M$  is mass of spacecraft,  $K$  is percentage of the sun as seen from spacecraft,  $\phi$  is solar flux at 1AU,  $c$  is speed of light,  $R_{AU}$  is distance between the spacecraft and Sun in AU, and  $\vec{a}$  is the acceleration vector in inertial coordinates.

### 3.3.4 Engine Models

The Astrogator allows the user to define the engine to be used in the spacecraft. The engine models available are constant thrust and specific impulse, Constant acceleration and specific impulse, and custom engine design.

#### 3.3.4.1 Constant Thrust and Specific Impulse

In this type of engine, the user specifies the thrust ( $F$ ) and specific impulse ( $I_{sp}$ ) value as a constant for the engine. Using these values the exhaust velocity ( $V_{exhaust}$ ) is calculated as,

$$V_{exhaust} = I_{sp} \times g \quad (3.5)$$

where, 'g' is the constant value of gravitational acceleration at Earth's sea level.

### 3.3.4.2 Constant Acceleration and Specific Impulse

In this type of engine, the user defines the acceleration and specific impulse as constant. The engine model during flight adjusts the thrust based on the change in spacecraft mass due to propellant consumption and to hold the constant acceleration and specific impulse value. The thrust is calculated as a function of time and is given by,

$$F(t) = \dot{m}(m(t), I_{sp}g, a) \times g \times I_{sp} \quad (3.6)$$

The mass flow rate is the function of exhaust velocity and thrust produced,

$$\dot{m} = \frac{F}{V_{exhaust}} \quad (3.7)$$

The default value of gravitational acceleration used in the model is 0.00980665 km/sec<sup>2</sup>.

### 3.3.5 B-Plane Targeting

The B-plane is a planar coordinate system that allows targeting of spacecraft for a gravity assist or orbit capture around a celestial body. The B-plane is defined to contain the focus of the spacecraft and central body's trajectory that is assumed to be hyperbola. The plane must also be perpendicular to the incoming spacecraft's trajectory asymptote [ref. Stephen]. Figure 3.1 below shows the B-plane between spacecraft trajectory and target planet.



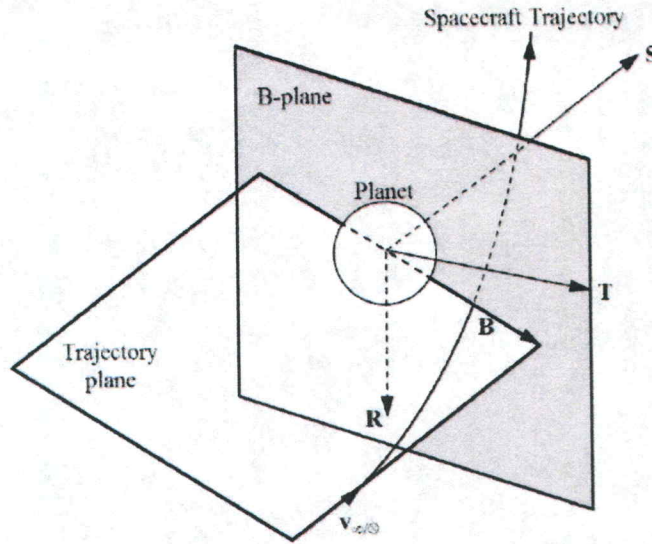


Figure 3.1 B-Plane geometry[72].

The Cartesian and polar components of the B-plane vectors are:

$$Cartesian = \begin{cases} B_T = \vec{B} \cdot \vec{T} \\ B_R = \vec{B} \cdot \vec{R} \end{cases}$$

$$Polar = \begin{cases} \theta = \tan^{-1} \left( \frac{B_R}{B_T} \right) \\ b \end{cases}$$

### 3.4 MCS Script Setup

The Astrogator MCS script is defined in sequence of components used to propagate spacecraft's trajectory. The description of the components is given below. The calculations used to determine spacecraft properties are mentioned in section 4.1.

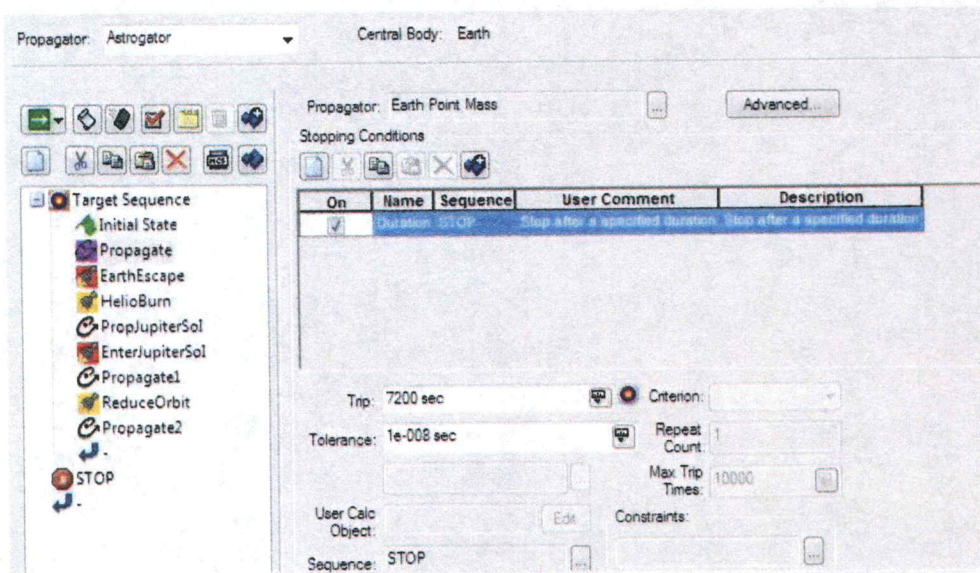


Figure 3.2 Screenshot of Astrogator GUI.

### 3.4.1 Spacecraft Configuration and Initial Elements

The Initial state segment is used to define the spacecraft configuration and initial elements of the spacecraft's orbit. The spacecraft parameters required to configure the segment are dry mass, drag area, drag coefficient, spherical radiation pressure and radiation pressure due to central body (Albedo/ thermal pressure). The spacecraft's fuel tank configuration requires the user to define fuel density, fuel mass, maximum fuel mass, tank pressure, volume and its nominal temperature. The fuel density value was defined as  $530 \text{ kg/m}^3$  based on the density of lithium.

#### 3.4.1.1 Coordinate System and Initial Orbital Elements

The spacecraft is initially assumed to be in Low Earth Orbit, to define the initial orbital elements, the first requirement is to select the central body reference frame. Every central body's coordinate systems originates at its center of mass and the only difference in every reference frame is the defined reference axes of each coordinate system. The frame

used to define initial elements is ‘Earth J2000’ which is defined by the mean epoch and mean equinox at the epoch of 1 Jan 2000 at 12:00:00.000 TDB. The J2000 reference frame is derived from the transformational algorithm which uses the 1980 nutation model[73], theory of Earth’s precession and mean obliquity.

The initial orbit is defined based on the coordinate type and orbital elements specified. The keplerian coordinate type is used to define the initial orbit size and shape. The required parameters are orbit epoch time, semimajor axis, eccentricity, argument of periapsis, inclination, longitude of the ascending node and true anomaly.

### 3.4.2 Propagate Segment

This propagate segment is used to propagate the spacecraft’s initial orbit as per the keplerian elements. The initial orbit defined is a 300 km circular orbit with 28.5 degree inclination. Earth point mass high-precision numerical two body orbit propagator is used during this segment. The stopping condition for this segment is the ‘duration’ of propagation which is specified for two hours. The numerical integrator properties for the 7<sup>th</sup> order Runge-Kutta-Fehlberg integrator[74] with 8<sup>th</sup> order error control are mentioned in table 3.2.

Table 3.2 Numerical integrator properties and step size control

Initial step size	60 seconds	Maximum absolute error	$1 \times 10^{-13}$
Maximum step	8400 seconds	Maximum relative error	$1 \times 10^{-13}$
Error control	Relative to state	Maximum iterations	100

### 3.4.3 Maneuver Segment for Earth Escape

The first maneuver segment in the mission control sequence is used to propel the spacecraft out of the central body’s SoI, in this case Earth being the central body. The



equations used to calculate the SoI for various planets are mentioned in the Appendix B. Table 3.3 shows the calculated values of SoI of each celestial body used in the trajectory models. During the maneuver segment, the pressure system in the fuel tank is considered to be regulated with constant pressure as the propellant mass decreases during the propulsion system run time.

Table 3.3 Calculated Sphere of Influence

Celestial Body	Radius of Sphere of Influence (km)
Earth	924,526
Earth's Moon	66,183
Jupiter	$48.6 \times 10^6$
Saturn	$54.5 \times 10^6$

The finite maneuver is used for the segment which propagates the trajectory while applying the acceleration due to thrust simultaneously. The attitude control of the vector is applied along the thrust vector and is updated during the burn. The thrust axes are aligned and constrained to position and velocity vector along trajectory of point relative to Earth inertial reference frame. The thrust vector axes are aligned as velocity (X-axis), Normal (Y-axis) and Co-Normal (Z-axis). The engine model used was with constant thrust and  $I_{sp}$  with Earth's surface gravity acceleration for  $I_{sp}$  conversion being  $0.0098 \text{ km/sec}^2$ . The Cislunar propagator is used during Earth escape maneuver segment which consists Earth's WGS84 gravitational model and Sun and Moon as third body effect. The stopping condition for the segment is defined by radius of Earth's SoI.

#### **3.4.4 Maneuver segment for heliocentric trajectory**

The maneuver segment for heliocentric trajectory involves the thrust axes to be in Sun inertial reference frame with velocity, Normal, Co-Normal axes with X-axis along velocity vector and Z-axis towards position vector. The attitude control is along the thrust vector and is updated during the burn. The engine model is constant thrust and  $I_{sp}$  with pressure regulated system. Heliocentric propagator is used during this segment which models two body force model with Sun being the central body and all the other planets in the solar system considered for third body effect. The stopping condition for this segment is 'duration' which needs to be iterated as per the mission requirement.

#### **3.4.5 Propagate Segment**

The propagate segment is used to propagate the spacecraft's trajectory to the target planet's SoI. The stopping conditions being the 'duration' and specified distance from the origin of the target celestial body. Heliocentric propagator model is used with Sun being the central body and all the other planets in the solar system acting as third body effect. The duration of the segment is iterated using target sequence to determine the correct duration of the segment.

#### **3.4.6 Maneuver segment for planetary approach**

Planetary approach phase uses maneuver segment to target the spacecraft towards the destination planet. The attitude control is set to anti-velocity vector to reduce spacecraft's heliocentric velocity and is updated during burn. High precision orbit propagator is used for target planet system. Sun and target body's moon act as third body effect in the propagator function. The stopping conditions are set to the periapsis and magnitude of distance set from the target body.

#### **3.4.7 Propagate segment before planetary orbital insertion**

Once the spacecraft achieves the stopping conditions defined in the previous maneuver segment, propagate segment is used to align the spacecraft before orbit insertion burn such as to define the first captured orbit using target body's high precision orbit propagator.

#### **3.4.8 Maneuver segment for orbital insertion**

The spacecraft performs the finite maneuver burn to reduce the velocity of the spacecraft in order to obtain the orbital insertion around the target planetary body. The duration of the burn depends on the minimum  $\Delta V$  requirement for the orbital capture and the desired initial orbit around the target planetary body.

#### **3.4.9 Maneuver segment for orbit changes and corrections**

Once the spacecraft completes the first captured orbit, the next orbit can be designed based on the mission objective. The maneuver type for this segment can be impulsive if spacecraft's onboard chemical propellants are to be used otherwise finite maneuver can be implemented using main engine for orbit correction. This segment is optional and is applicable to only as per mission operational requirement. The thrust vector can be defined in Cartesian or spherical coordinates for attitude control. The stopping condition is the time duration based on the attitude control requirements.

#### **3.4.10 Propagate segment for science mission**

Once the spacecraft is in its final desired orbit, the propagate segment can be used to define the orbit based on the time duration to conduct the science experiments. Based on



the desired final orbit, this segment can be implemented using simple numerical two body propagation or high precision orbit propagator.

### 3.4.11 Target sequence

The target sequence is used define the control parameters of maneuvers and propagation segment. The complete mission control sequence is nested under the target control sequence. The two differential corrector profile created to determine dependent variables are inclination and B-plane computation of the target planet. Table 3.4 mentions the control parameters to obtain desired inclination and B-plane parameters.

Table 3.4 Control parameters to obtain desired inclination and B-plane parameters

Orbit epoch	Thrust axes during heliocentric maneuver
RA of outgoing asymptote	Cruise phase duration
Declination of outgoing asymptote	Thrust axes during orbit insertion

### 3.4.12 Stop segment for mission conclusion

Finally, Stop segment is used at the end of the mission to conclude the mission control sequence.

## **CHAPTER 4. MISSION DESIGN**

The objective of the mission design is to perform a rendezvous mission to gas giant planets using a nuclear fusion propulsion spacecraft. Spacecraft's trajectory phases are described in section 4.1. The spacecraft design parameter calculations are explained in section 4.2 and trajectory analysis for rendezvous mission to Jupiter is demonstrated in section 4.3, and section 4.4 demonstrates the rendezvous mission to Saturn.

### **4.1 Trajectory Analysis for Planetary Escape and Capture**

The trajectory for the fusion propulsion spacecraft is designed in three phases, the acceleration phase, coasting phase and orbital insertion phase. The initial parking orbit of the spacecraft has been selected to be in circular low Earth orbit at 300 km altitude with 28.5 degrees of inclination so as to use the maximum payload capacity of the launch vehicle considering the launch to be from Kennedy Space Center, Florida.

#### **4.1.1 Earth Escape and Acceleration Phase**

During the Earth escape and acceleration phase the thrust vector is along the Velocity Normal Co-Normal (VNC) axes with X-axis along velocity vector, Y-axis is along the orbit normal and Z-axis completes the orthogonal triad. During the first finite burn, the spacecraft uses the continuous thrust, spiral trajectory phase starting from the initial parking orbit until it reaches Earth sphere of influence. The calculated Earth Sol uses,

$$R_{SOI} = a \left( \frac{M_{ob}}{M_{pb}} \right)^{2/5} \quad (4.1)$$

giving  $R_{SOI} = 924,526$  km.

Due to the close vicinity of Moon's orbit, the spacecraft uses the CisLunar propagator as the force model during its continuous thrust spiral orbits around Earth which consists of WGS84 gravitational model of Earth and the effect of Moon and Sun as the third body.

In the second finite burn after spacecraft exits Earth's SoI, the spacecraft uses the heliocentric propagator as a force model with the Sun being the central body and all the other planets having the third body effect. The thrust axes are along the VNC axes with sun inertial being the reference system. The time duration for the finite burn is decided with respect the  $\Delta V$  requirement for the target celestial body.

#### **4.1.2 Coasting Phase**

During this phase the propulsion system is turned off and heliocentric propagator model is used. The spacecraft coasts along the heliocentric trajectory and decelerates continuously due to the Sun's gravitational influence.

#### **4.1.3 Planetary Approach and Orbital Insertion Phase**

During this phase the spacecraft's heliocentric velocity is reduced by pointing the thrust vector opposite to the spacecraft's inertial velocity vector. The propagator model used during this phase would have the target planet as the central body along with the Sun and target planet's moons for the third body effect. The stopping conditions for the spacecraft's propulsion system will be the specified distance from the target body's origin and its periapsis.



## 4.2 Spacecraft Design

The spacecraft designed for the trajectory analysis has been optimized with respect to the payload carrying capacity of NASA's future heavy lift launch vehicle Space Launch System (SLS) Block-2 Cargo[75]. The destination planet's for rendezvous mission are chosen to be Jupiter and Saturn because the spacecraft's trajectory can be compared with the ongoing robotic Juno mission to Jupiter and recently concluded Cassini-Huygens mission to Saturn. The spacecraft has been designed in a way that it should be delivered in Low Earth Orbit by SLS in a single launch. The evolved SLS Block-2 Cargo vehicle will have payload delivering capacity of more than 130 mT to LEO with 1800 cubic meters of payload volume[76]. Thus, the maximum mass of the designed spacecraft is constraint to 120 mT.

Some of the spacecraft design parameters are predetermined based on previous literature studies such as payload mass ratio, specific power and subsystem mass[40], [77]. The first predetermined parameter is the payload mass ratio ( $\lambda$ ). The payload mass ratio for a spacecraft is defined as the payload mass divided by the difference in total mass and payload mass. The value of 0.263 and 0.142 for Jupiter and Saturn respectively has been used for a fusion propulsion rendezvous mission. The second predetermined parameter is the specific power, denoted by  $\alpha$ . A minimum specific power of 1 kW/kg has been selected considering it to be developed for the early technology demonstration. The other predetermined parameters are the mass values. For  $\lambda=0.263$ , the payload mass calculated for Jupiter rendezvous mission is about 25 mT and with  $\lambda=0.142$ , the payload mass calculated for Saturn rendezvous mission is about 15 mT. The mass for main propulsion system has been constrained to 30 mT. With the above calculated values, the remaining

mass is allocated to structure (includes power system, avionics, attitude thrusters) and main propulsion propellant. Table 4.1 shows the spacecraft dry mass breakdown for the rendezvous mission to Jupiter. The validity of the determined values must be reevaluated as the design for an actual fusion propulsion powered spacecraft progresses.

Table 4.1 Spacecraft dry mass breakdown

System	Mass, mT
Payload (Jupiter mission)	25
Payload (Saturn mission)	15
Structure	35
Main propulsion system	30

The approximate trip time for rendezvous mission is calculated using the field-free equation which requires specific power and payload mass ratio[77]. Also, the straight line distance (R) from Earth to the destination planet is used in the equation.

$$t_{trip} = \frac{3}{2} \left[ \frac{2R \sqrt{\frac{1}{2\alpha}}}{1 - \sqrt{\lambda}} \right]^{\frac{2}{3}} \quad (4.2)$$

where  $t_{trip}$  is the total trip time, R is the straight line distance between Earth and destination Planet,  $\alpha$  is the specific power in kW/kg, and  $\lambda$  is the payload mass fraction.

The straight line distance in the trajectory analysis includes both the average distance from the Sun to Earth and the average distance from Sun to the destination planet. The reason is that the Earth will always be on the opposite side of the Sun from the destination planet's position when the spacecraft begins its mission. Using equation 4.2, the approximate trip time to Jupiter is 336.1 days. It should be noted that the trip time

calculated here uses gravity free equations of motion and does not include missions which enter or depart from low orbits. It is estimated that in order to achieve the shortest trip time, about 70% of the overall trip time will include Earth departure, heliocentric acceleration and deceleration during planetary approach and orbital insertion which would require continuous run of fusion propulsion system. The 30% trip time is assumed to consist of the coasting phase in heliocentric trajectory. With this assumption, the fusion propulsion run time during heliocentric trajectory becomes 235 days. Also, since the spacecraft departs from Low Earth Orbit, the time approximated for the spacecraft to escape the Earth's SoI is 25 days. Thus, the total run time of fusion propulsion from Low Earth Orbit to the destination planet is 260 days.

Using the equations derived from the definition of specific power and jet power, the specific impulse can be calculated.

The specific power is given by,

$$\alpha = \frac{P_{jet}}{m_{ps}} \quad (4.3)$$

where  $\alpha$  is the specific power in W/kg,  $P_{jet}$  is the jet power in W and  $m_{ps}$  is the mass of the propulsion system in kg.

$$P_{jet} = \frac{1}{2} \dot{m} V_e^2 \quad (4.4)$$

where  $P_{jet}$  is the jet power in W,  $\dot{m}$  is the mass flow rate in kg/s and  $V_e$  is the engine exhaust velocity in m/s.

$$I_{sp} = \frac{V_e}{g_o} \quad (4.5)$$

where  $I_{sp}$  is the specific impulse in seconds,  $V_e$  is the engine exhaust velocity in m/s and  $g_o$  is the Earth surface gravity acceleration constant, 9.806 m/sec<sup>2</sup>



The specific impulse is also given by,

$$I_{sp} = \frac{1}{g_o} \sqrt{2\alpha t_r} \quad (4.6)$$

where  $I_{sp}$  is the specific impulse in seconds,  $\alpha$  is the specific power in kW/kg,  $g_o$  is the Earth surface gravity acceleration constant, 9.806 m/sec<sup>2</sup> and  $t_r$  is the propulsion system run time in days.

The specific impulse calculated from equation 4.6 is 22,505.32 seconds. This value was rounded down to 22,500.0 seconds and used as an engine parameter for trajectory analysis. The value of specific impulse is then used to determine the exhaust velocity which is given by,

$$V_e = g_o I_{sp} \quad (4.7)$$

where  $V_e$  is the engine exhaust velocity in m/s,  $I_{sp}$  is the specific impulse in seconds and  $g_o$  is the Earth surface gravity acceleration constant, 9.806 m/sec<sup>2</sup>

The exhaust velocity calculated from equation 4.7 is 220,649.6 m/s. This value is used in the calculation of mass flow rate as,

$$\dot{m} = \frac{2\alpha m_{ps}}{V_e^2} \quad (4.8)$$

where  $\dot{m}$  is the mass flow rate in kg/s,  $\alpha$  is the specific power in kW/kg,  $V_e$  is the engine exhaust velocity in m/s and  $m_{ps}$  is the mass of the propulsion system in kg.

The mass flow rate calculated from equation 4.8 is 0.0012 kg/s. Now, using the mass flow rate and the exhaust velocity, we can calculate the thrust generated by the designed fusion propulsion system. The equation to determine thrust is given by,

$$F = \dot{m} V_e \quad (4.9)$$

where  $F$  is the thrust in newtons,  $\dot{m}$  is the mass flow rate in kg/s and  $V_e$  is the engine exhaust velocity in m/s.

The thrust value calculated from the equation 4.9 is 271.96 N. This value is rounded down to 272 N and is used as a spacecraft engine parameter for the trajectory analysis. The updated mass flow rate with thrust of 272 N is 0.0012 kg/s.

The approximate total propellant required for the mission can be determined based on the propulsion system run time and mass flow rate.

$$m_p = \dot{m}t_r \quad (4.10)$$

where,  $m_p$  is the propellant mass in mT,  $\dot{m}$  is the mass flow rate in kg/s and  $t_r$  is the propulsion system run time in days.

The calculated propellant requirement for the mission using equation 4.10 is 27,691 kg. This value was rounded down to an increased value of 30,000 kg (30 mT) for trajectory calculations which would apply gravity models.

Using the above calculated parameters, the empty mass of the spacecraft can be calculated as,

$$m_e = \frac{1}{\lambda} m_{pl} - m_p \quad (4.11)$$

where  $m_e$  is the spacecraft empty mass in mT,  $\lambda$  is the payload mass fraction,  $m_{pl}$  is the payload mass in mT and  $m_p$  is the total propellant mass in mT.

The calculated spacecraft empty mass from the equation 4.11 is 65.05 mT. This value is rounded down to 65 mT for the trajectory analysis. The empty mass and the payload mass of the spacecraft together make it as a dry mass of the spacecraft. Thus, the dry mass calculated is 90 mT. The initial mass of the spacecraft can be determined by

adding spacecraft dry mass and total propellant mass. Using both the values, initial mass of the spacecraft is calculated to be 120 mT.

Table 4.2 below provides the summary of predetermined parameters and calculated parameters of the spacecraft for Jupiter rendezvous mission.

Table 4.2 Spacecraft design parameters for Jupiter rendezvous mission

Predetermined parameters		Propulsion parameters		Mass, mT	
$\alpha$	$1 \frac{kW}{kg}$	$t_r$	260 days	$m_p$	30 mT
$\lambda_{Jupiter}$	0.263	$V_e$	220,649.6 m/s	$m_e$	65 mT
$m_{pl(Jupiter)}$	25 mT	$\dot{m}$	0.0012 kg/s	$m_{dry}$	90 mT
		$I_{sp}$	22,500 seconds	$m_i$	120 mT
		F	272 N		

Similarly, the spacecraft parameters for Saturn rendezvous mission were calculated. The calculated trip time was 406 days. Using this value, the fusion propulsion run time was calculated to be approximately 309 days. The main propellant requirement increases with increase in propulsion system run time. Thus, the maximum payload carrying capacity was determined to be about 15 mT. Apart from these values, the other propulsion parameters of the spacecraft were kept constant.

Table 4.3 below provides the summary of predetermined parameters and calculated parameters of the spacecraft for Saturn rendezvous mission.



Table 4.3 Spacecraft design parameters for Saturn rendezvous mission

Predetermined parameters		Propulsion parameters	Mass, mT
$\alpha$	$1 \frac{kW}{kg}$	$t_r$ 309 days	$m_p$ 40 mT
$\lambda_{Jupiter}$	0.142	$V_e$ 220,649.6 m/s	$m_e$ 65 mT
$m_{pl(Jupiter)}$	15 mT	$\dot{m}$ 0.0012 kg/s	$m_{dry}$ 80 mT
		$I_{sp}$ 22,500 seconds	$m_i$ 120 mT
		F 272 N	

### 4.3 Jupiter Rendezvous Mission

The spacecraft will begin its mission with orbit epoch of 7 April 2034 at 12:00:00:000 UTCG. As stated in the previous section, that spacecraft's initial orbit will be at circular in 300 km altitude. The initial state orbital elements of the spacecraft are mentioned in table 4.4.

Table 4.4 Initial state orbital elements

Elements	Defined parameters
Coordinate System	Earth J2000
Coordinate type	Keplerian
Orbit epoch	7 Apr 2034 12:00:000 UTCG
Element type	Osculating
Semi-major axis	6678.14 km
Eccentricity	0
Inclination	28.5 deg.
Right Asc. Of Asc. Node	0 deg.
Argument of Periapsis	0 deg.
True Anomaly	360 deg.

Based on the initial state orbital elements, the spacecraft is propagated considering Earth as point mass with a stopping condition duration of 120 min. This phase is used to verify the spacecraft's initial parking orbit and prepare the spacecraft for Earth departure phase. After this segment, the spiral out Earth escape segment maneuver is initiated. The direction of the thrust is along Velocity – Normal - Co-normal (VNC) coordinate frame relative to Earth and spacecraft. In VNC coordinate frame, the X-axis is along the velocity vector ( $\vec{V}$ ), the Y-axis is along the orbit normal ( $Y = \vec{R} \times \vec{V}$ ) and the Z- axis completes the orthogonal triad ( $Z = X \times Y$ ). The complete thrust is along the velocity vector of the spacecraft so as to maximize the required  $\Delta V$  for Earth escape. The fusion propulsion system during this segment runs for a total duration of  $3.41272 \times 10^6$  sec. The maneuver direction with respect to the VNC (Earth) frame is updated during the thrust period. The

thrust efficiency of the propulsion system is considered to be nominal with the value of 1. The thrust efficiency is related to the final thrust and the engine thrust produced by the propulsion system.

$$F_{final} = \eta F_{engine} \quad (4.12)$$

where  $\eta$  is the thrust efficiency,  $F_{final}$  is the final thrust and  $F_{engine}$  is the engine thrust.

The mass flow rate of the engine during maneuver segment remains constant throughout the mission with the value of 0.0012 kg/s. The  $\Delta V$  magnitude and fuel used at the end of spiral out acceleration phase maneuver segment are 7.87 km/sec and 4206.94 kg respectively. Figure 4.1 and Figure 4.2 shows the trajectory of the spacecraft's Earth escape from epoch.

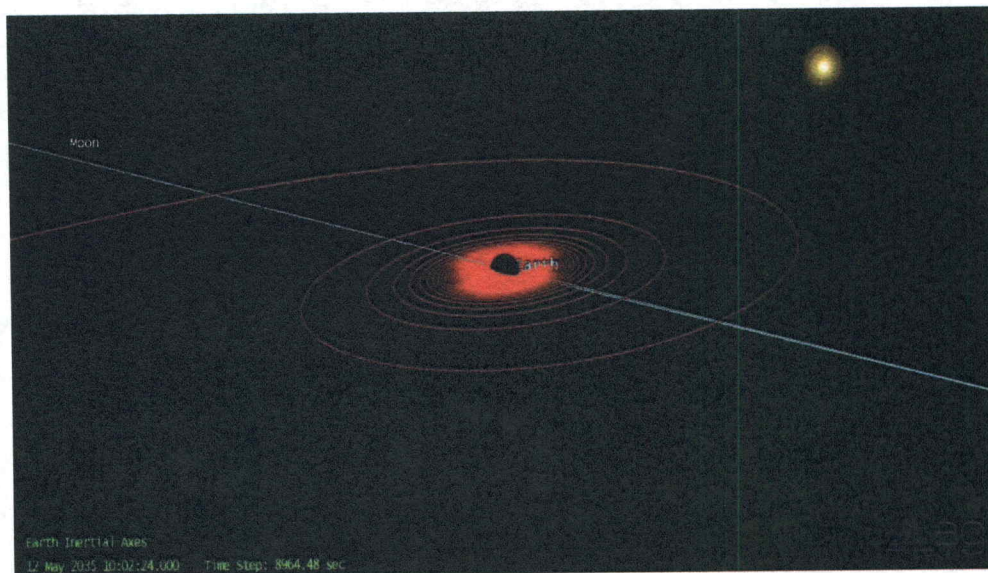


Figure 4.1 3D trajectory of spacecraft transfer from LEO to Earth escape



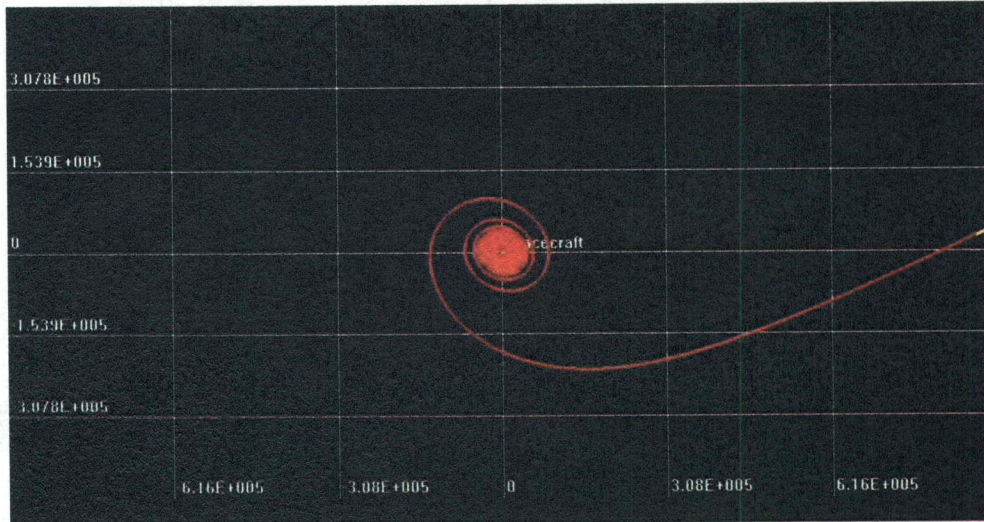


Figure 4.2 2D trajectory of spacecraft transfer from LEO to Earth escape

The spacecraft's distance during the Earth escape maneuver phase is shown in the figure 4.3. The maneuver segment stops once the spacecraft reaches the Earth's SoI radius of 924,526 km. Figure 4.4 shows the total fuel consumption during this segment.

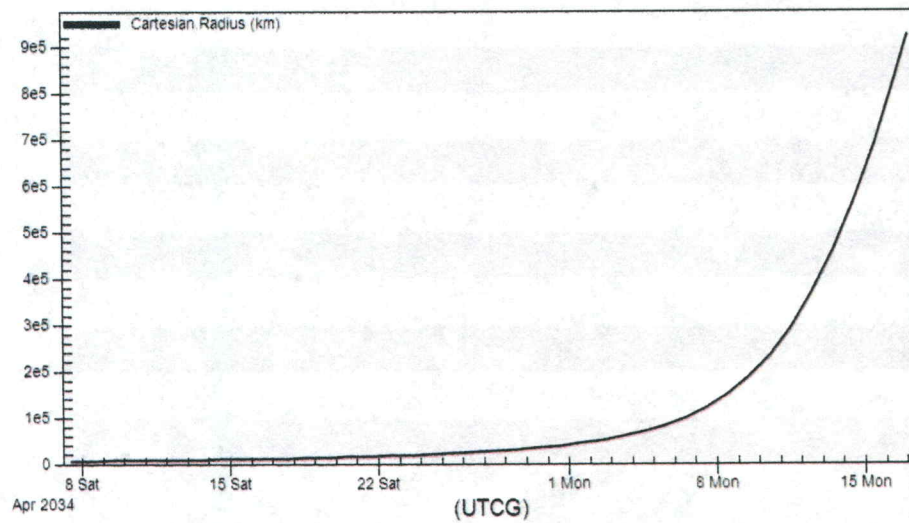


Figure 4.3 Spacecraft distance during Earth escape maneuver segment

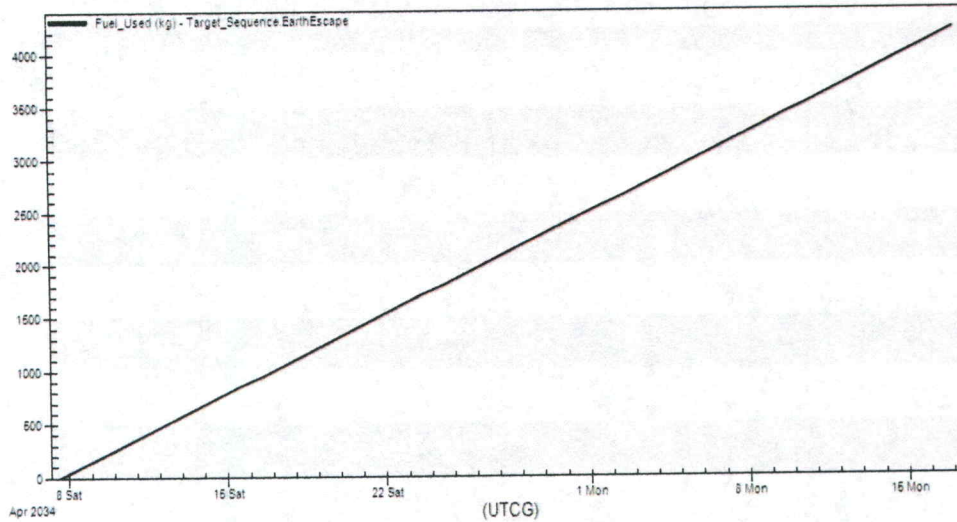


Figure 4.4 Fuel used during Earth escape maneuver segment

The specific impulse and thrust magnitude of the spacecraft during this phase are as per the designed parameter of 22,500 seconds and 272N respectively.

Once the spacecraft completes the maneuver segment for Earth escape, it has obtained the characteristic energy (C3) of 3.27 km<sup>2</sup>/sec<sup>2</sup>. The minimum C3 energy required for a spacecraft to escape Earth's gravitational influence is 0. Figure 4.7 shows the increment in C3 from Earth's LEO to Earth's SoI radius.

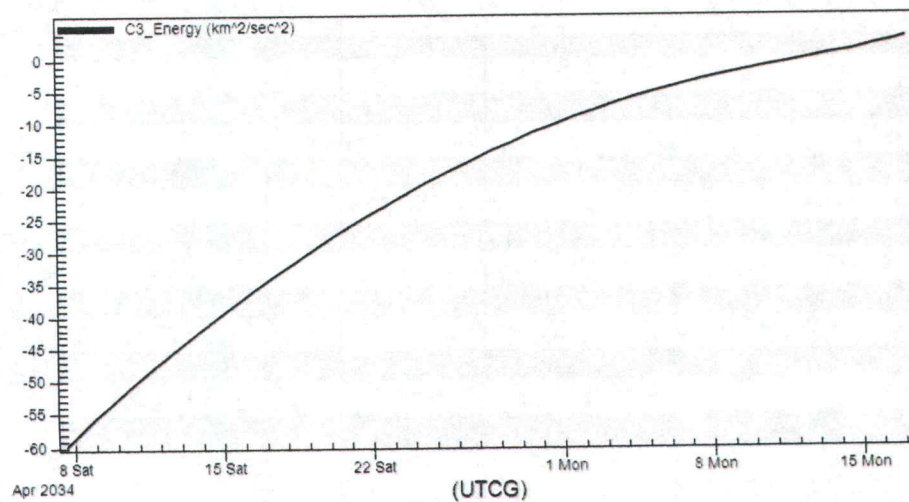


Figure 4.5 Spacecraft C3 energy during Earth escape phase

The spacecraft now enters the heliocentric trajectory and is no more under the influence of Earth-Moon gravitational force. Now, the spacecraft will be provided with the extra energy and plane change for targeting Jupiter system. The orbital inclination of Jupiter with respect to Earth is 1.304 degrees[78] in J2000 ecliptic reference frame. The maneuver segment in heliocentric trajectory is defined as HelioBurn. The start time for the HelioBurn maneuver segment is on 17 May 2034 at 01:58:38.436 UTCG with total duration of this segment being  $8.64 \times 10^6$  sec. The thrust axes are along the VNC coordinate frame relative to Sun and spacecraft. The maneuver control parameters for HelioBurn segment are shown in table 4.5.

Table 4.5 HelioBurn maneuver segment parameters

Elements	Defined parameters
Maneuver type	Finite
Attitude Control	Thrust vector
Attitude update	Update during burn
Thrust axes	VNC (Sun)
X-axis (Velocity)	0.984808
Y-axis (Normal)	0
Z-axis (Co-Normal)	-0.173648
Propagator	Heliocentric

The  $\Delta V$  magnitude during this segment is 21.29 km/sec and the spacecraft has consumed 10650.73 kg of fuel leaving 15142.3 kg of fuel left inside the main propellant tank. The trajectory of the spacecraft in heliocentric phase from epoch to the final burn of HelioBurn maneuver segment is shown in Figure 4.8 and Figure 4.9.



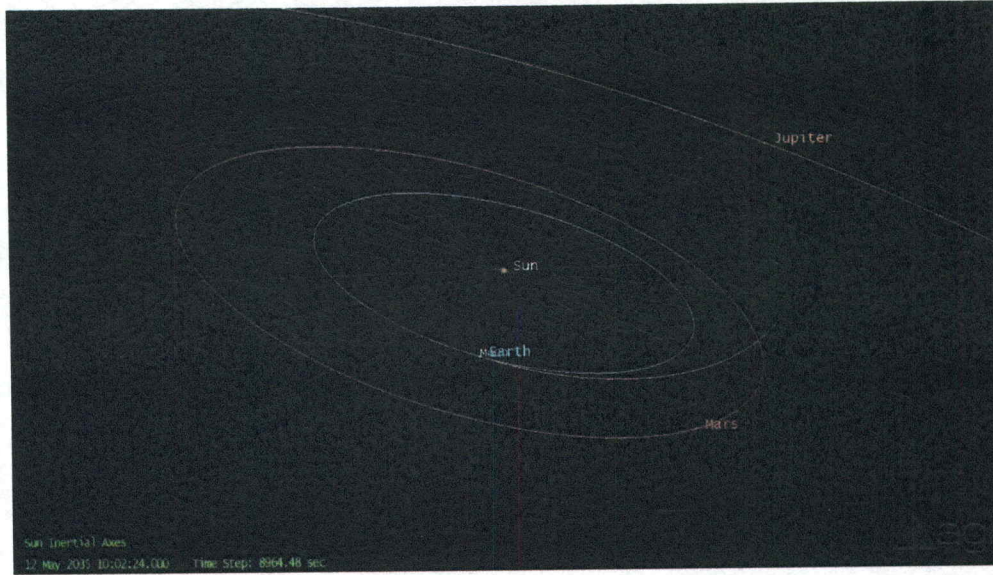


Figure 4.6 3D trajectory of spacecraft transfer from epoch to the final HelioBurn

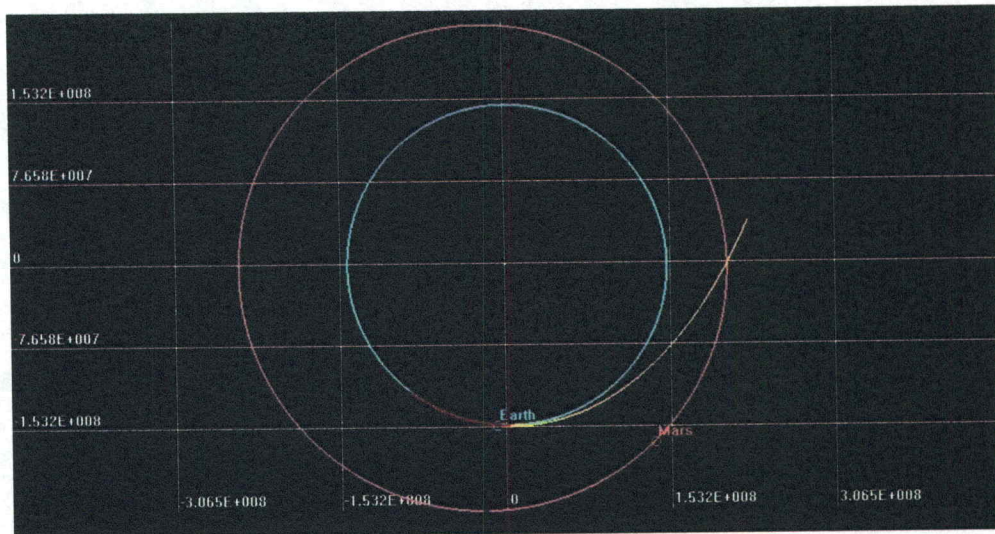


Figure 4.7 2D trajectory of spacecraft transfer from epoch to the final HelioBurn

On completion of this segment, the main thruster is turned off on 25 Aug 2034 at 01:58:38.435 UTCG. At this point, the position of the spacecraft in Sun J2000 reference frame are -207656643.29 km in X-direction, 90199488.36 km in Y-direction and 42803806.63 km in Z-direction. Thus, the magnitude distance of the spacecraft from Sun

is about 230411360.54 km. Figure 4.10 shows the distance of the spacecraft from epoch to the completion of HelioBurn maneuver segment in Sun J2000 reference frame.

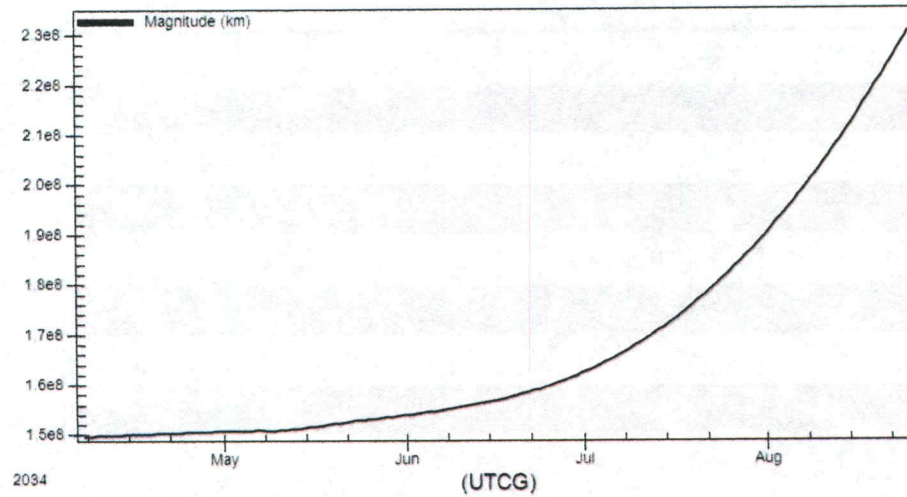


Figure 4.8 Spacecraft's distance from epoch to the final burn of HelioBurn maneuver segment in Sun J2000 reference frame

The final C3 energy achieved at the end of the HelioBurn is 522.87 km<sup>2</sup>/sec<sup>2</sup>. Figure 4.11 shows the increment in C3 energy from epoch till the end of HelioBurn segment.

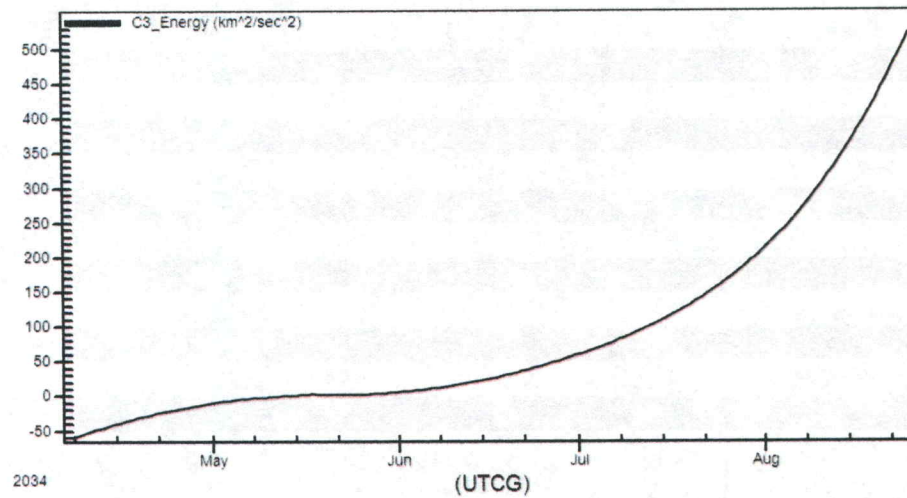


Figure 4.9 Spacecraft's C3 energy from epoch to the final burn of HelioBurn maneuver

After the completion of HelioBurn, the propulsion system switches from acceleration phase to coasting phase. During this segment, the spacecraft simply propagates



towards Jupiter system in heliocentric trajectory. The coasting segment is shown in Figure 4.12 and Figure 4.13.



Figure 4.10 3D trajectory of spacecraft transfer from epoch to the coasting phase

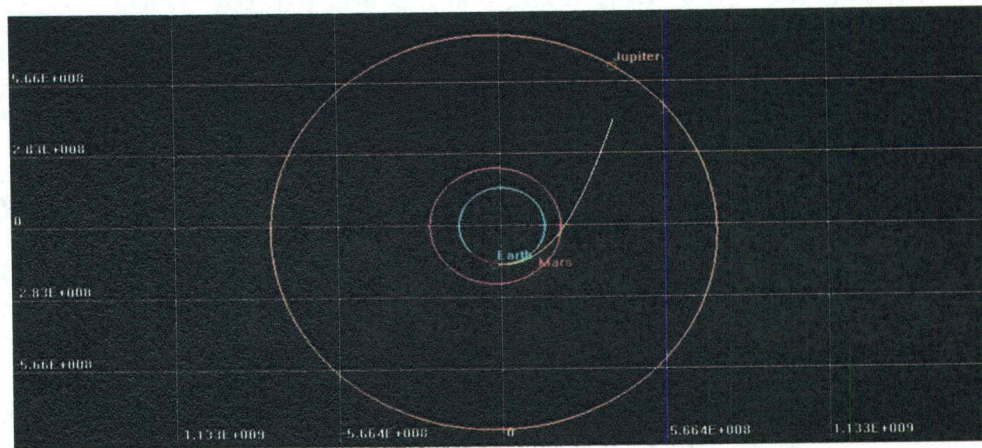


Figure 4.11 2D trajectory of spacecraft transfer from epoch to the coasting phase

The start time for the coasting phase is on 25 Aug 2034 at 01:58:38.436 UTCG which continues till 12 Jan 2035 at 01:58:38.436. Thus, the total duration of this phase is  $1.20 \times 10^7$  sec. After the completion of coasting phase, the spacecraft begins its maneuver



segment for Jupiter approach and orbit insertion phase. The spacecraft is now required to reduce its heliocentric velocity so that it can achieve orbit insertion with the help of Jupiter's gravity. This requires the spacecraft to provide thrust in negative velocity vector, which can be achieved by rotating the spacecraft in 180 degrees and continuously update the thrust vector during the propulsion system run time. Now that the spacecraft is near the Jupiter's SoI, the propagator used during this maneuver segment is Jupiter high precision orbit propagator which includes the third body effect of Sun, and major satellites of Jupiter such as Ganymede, Europa, Io and Callisto.

The start time for the Jupiter approach maneuver segment is on 12 Jan 2035 at 01:58:38.436 UTCG with total duration of this segment being  $1.03 \times 10^7$  sec. The  $\Delta V$  magnitude during this segment is 28.60 km/sec and has consumed 12780.87 kg of fuel leaving 2361.45 kg of fuel left inside the main propellant tank to be used for orbit correction maneuvers after spacecraft's orbit insertion. The maneuver segment for Jupiter approach and orbit insertion phase is shown in Figure 4.14 and 4.15.

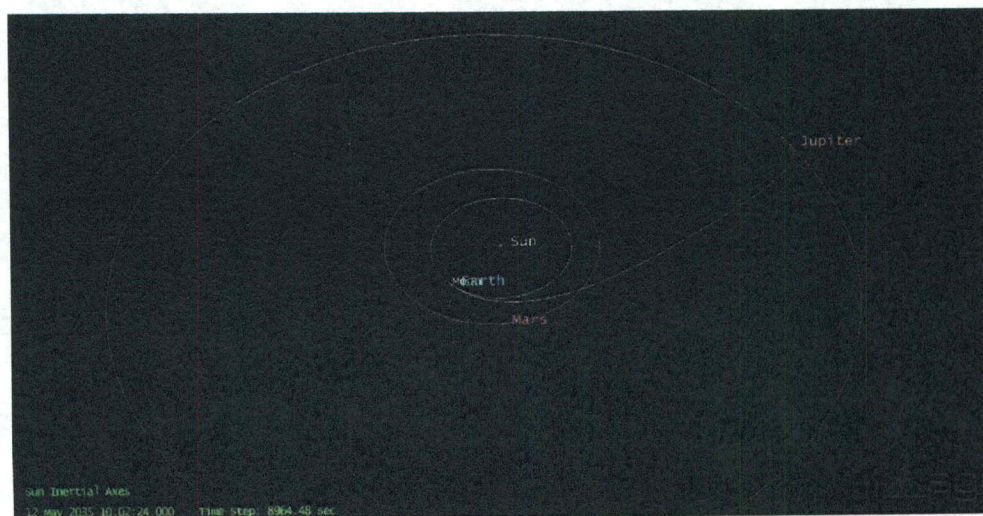


Figure 4.12 3D trajectory of spacecraft transfer from epoch JOI

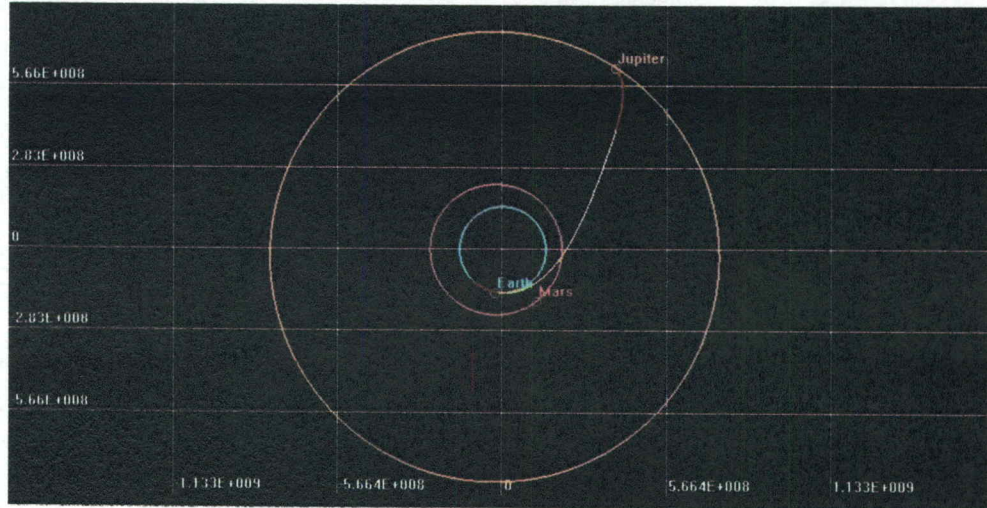


Figure 4.13 2D trajectory of spacecraft transfer from epoch JOI

The spacecraft's captured orbit with approximate orbital period of 21 days is shown in Figure 4.16.

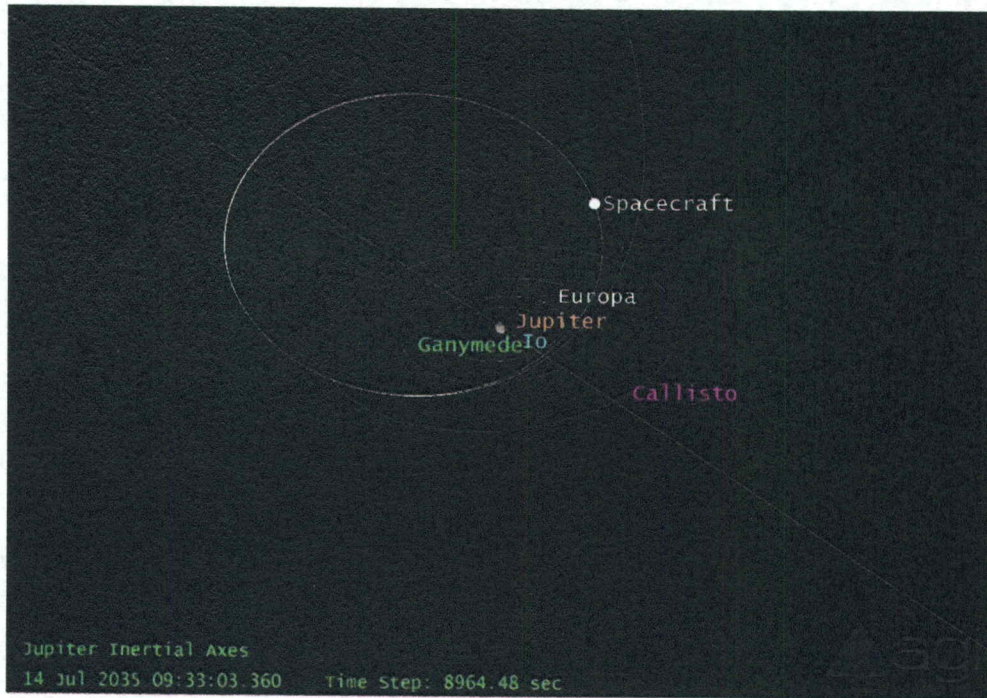


Figure 4.14 Spacecraft's captured orbit around Jupiter

The spacecraft's velocity during Jupiter approach phase and after orbit insertion is shown in Figure 4.17.



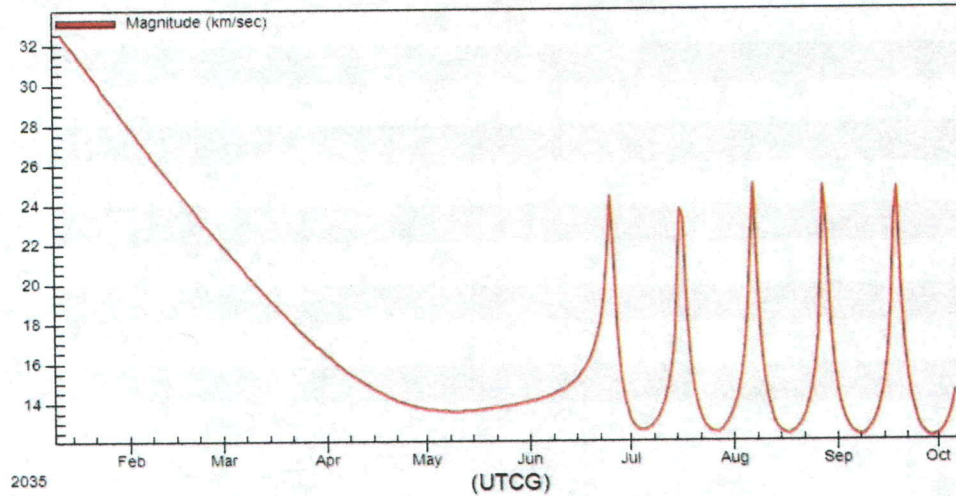


Figure 4.15 Spacecraft's velocity during Jupiter approach phase and JOI

After the spacecraft has achieved the orbit capture around Jupiter, a propagate segment is used to propagate the spacecraft's captured orbit for the next 100 days with Jupiter's high precision orbit propagator. Finally, stop segment is used to terminate the mission. The summary of Jupiter rendezvous mission timeline of is shown in table 4.6.

Table 4.6 Jupiter rendezvous mission timeline

Mission Phase	Duration (days)
Initial state	0
Earth escape phase	39 days
Acceleration phase (Thrust On)	39 days
Acceleration phase (Thrust Off)	139 days
Coasting phase	279 days
Jupiter approach phase (Thrust On)	279 days
Jupiter approach phase (Thrust Off)	399 days
Coasting	439 days
JOI and Orbit correction	446 days



#### 4.4 Saturn Rendezvous Mission

The spacecraft will begin its mission with orbit epoch of 26 July 2034 at 10:00:00:000 UTCG. The initial state orbital elements of the spacecraft are mentioned in table 4.7.

Table 4.7 Initial state orbital elements

Elements	Defined parameters
Coordinate System	Earth J2000
Coordinate type	Keplerian
Orbit epoch	26 Jul 2034 10:00:000 UTCG
Element type	Osculating
Semi-major axis	6678.14 km
Eccentricity	0
Inclination	28.5 deg.
Right Asc. Of Asc. Node	0 deg.
Argument of Periapsis	0 deg.
True Anomaly	360 deg.

Based on the initial state orbital elements, the spacecraft is propagated for 120 minutes using high precision orbit propagator with Earth as central body. After this segment, the spiral out Earth escape segment maneuver is initiated. The direction of the thrust is along the velocity vector of the spacecraft in VNC coordinate frame in order to maximize the required  $\Delta V$  for Earth escape. The fusion propulsion system during this segment runs for a total duration of  $3.41 \times 10^6$  sec. It can be noted that the Earth escape time is same as that of Jupiter rendezvous mission due to the same initial mass and orbit

specifications of the spacecraft. The maneuver direction with respect to the VNC (Earth) frame is updated during the thrust period with the thrust efficiency of 1. The mass flow rate of the engine during maneuver segment remains constant throughout the mission with the value of 0.0012 kg/s. The  $\Delta V$  magnitude and fuel used at the end of spiral out acceleration phase maneuver segment is 7.87 km/sec and 4206.94 kg respectively. Figure 4.18 and Figure 4.19 shows the trajectory of the spacecraft's Earth escape from epoch.

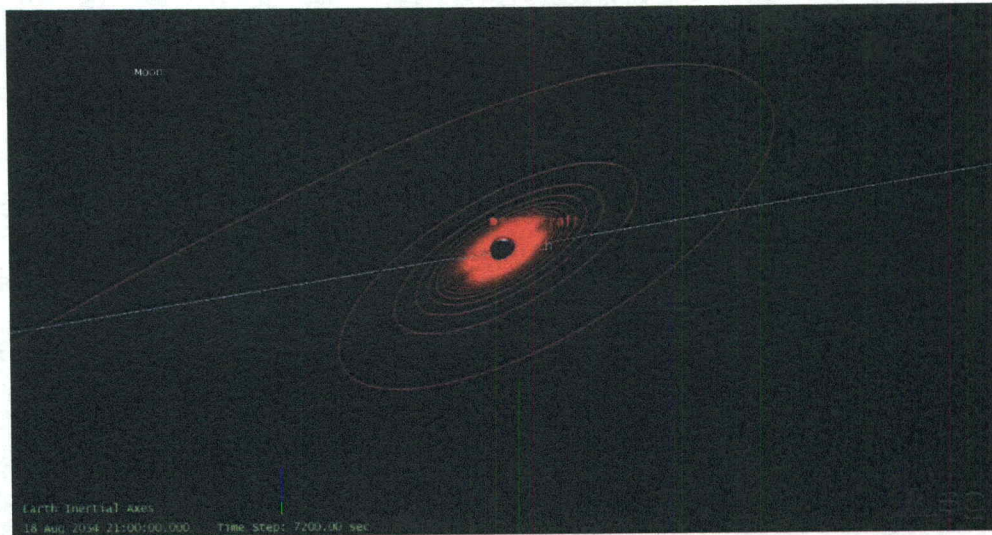


Figure 4.16 3D trajectory of spacecraft from LEO to Earth escape

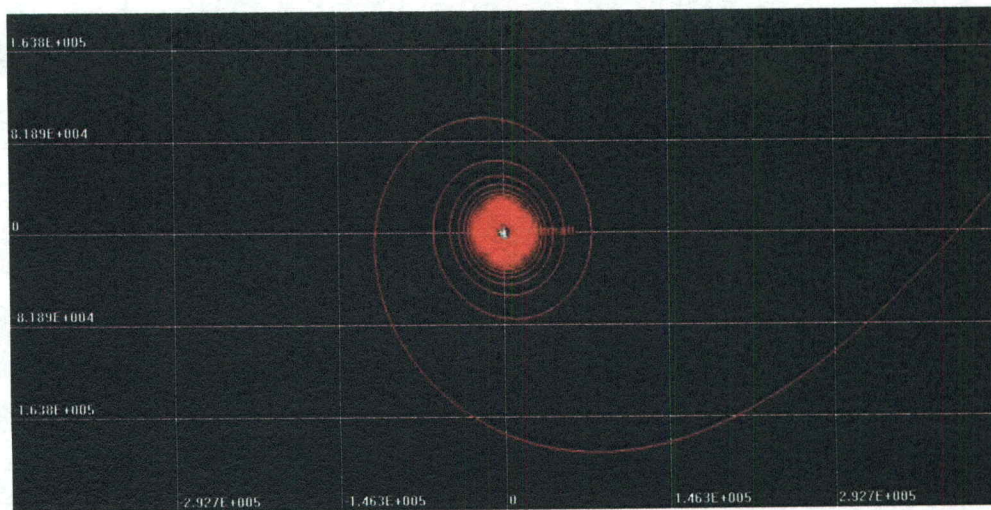


Figure 4.17 2D trajectory of spacecraft from LEO to Earth escape



The spacecraft's distance during the Earth escape maneuver phase is shown in the Figure 4.20. The maneuver segment stops once the spacecraft reaches the Earth's SoI radius of 924,526 km. Figure 4.21 shows the total fuel consumption during this segment.

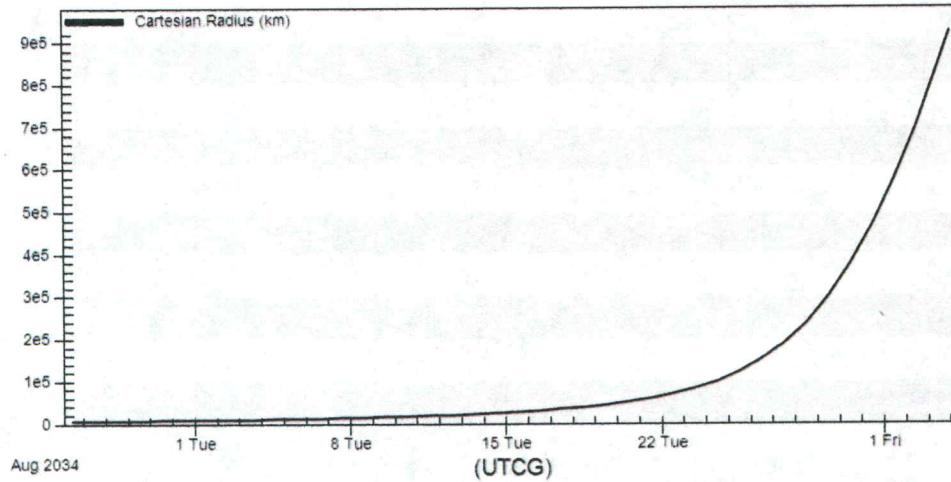


Figure 4.18 Spacecraft distance magnitude during Earth escape maneuver segment

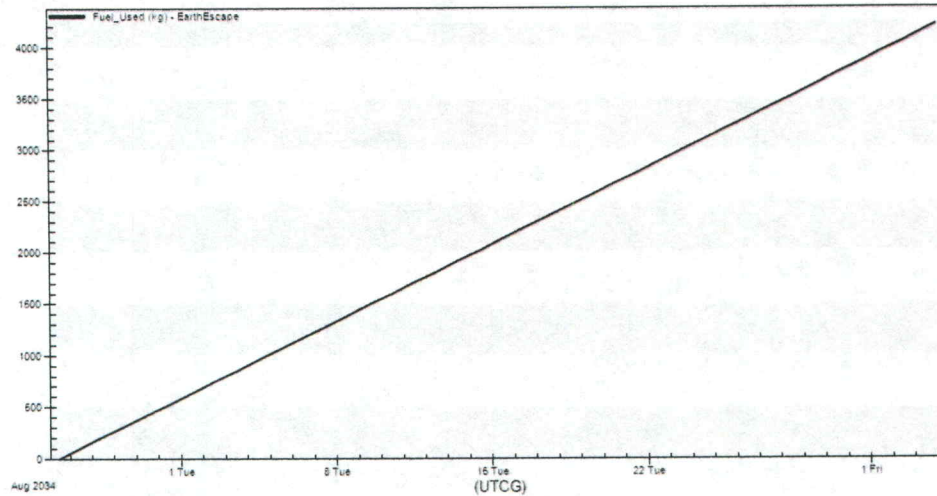


Figure 4.19 Fuel used during Earth escape maneuver segment

The specific impulse and thrust magnitude of the spacecraft during this phase are as per the designed parameter of 22,500 seconds and 272N respectively.



Once the spacecraft completes the maneuver segment for Earth escape, it has obtained the characteristic energy ( $C_3$ ) of  $3.18 \text{ km}^2/\text{sec}^2$ . Figure 4.24 shows the increment in  $C_3$  from Earth's LEO to Earth's SoI radius.

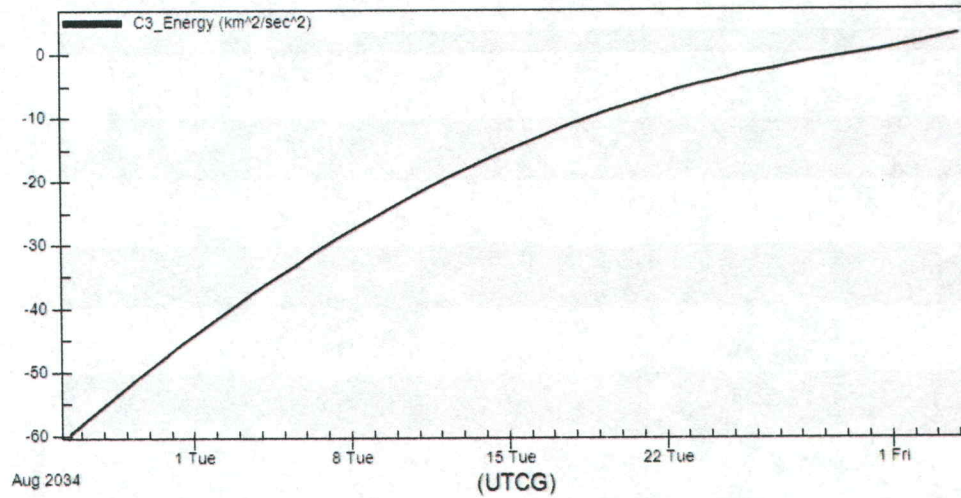


Figure 4.20 Spacecraft's C3 energy during Earth escape maneuver

The spacecraft now enters the heliocentric trajectory and is no more under the influence of Earth-Moon gravitational force. Now, the spacecraft will be provided with the extra energy and plane change for targeting Saturn system. The orbital inclination of Saturn with respect to Earth is 2.485 degrees[79] in J2000 ecliptic reference frame. The maneuver segment in heliocentric trajectory is defined as HelioBurn. The start time for the HelioBurn maneuver segment is on 4 Sep 2034 at 00:31:22.794 UTCG with total duration of this segment being  $1.32 \times 10^7$  sec. The thrust axes are along the VNC coordinate frame relative to Sun and spacecraft. The maneuver control parameters for HelioBurn segment are shown in table 4.8.

Table 4.8 HelioBurn maneuver segment parameters

Elements	Defined parameters
Maneuver type	Finite
Attitude Control	Thrust vector
Attitude update	Update during burn
Thrust axes	VNC(Sun)
X-axis (Velocity)	0.994532
Y-axis (Normal)	0
Z-axis (Co-Normal)	-0.104528
Propagator	Heliocentric

The  $\Delta V$  magnitude during this segment is 33.63 km/sec and has consumed 16370.17 kg of fuel leaving 24420.5 kg of fuel left inside the main propellant tank. The trajectory of the spacecraft in heliocentric phase from epoch to the final burn of HelioBurn is shown in Figure 4.25 and Figure 4.26.

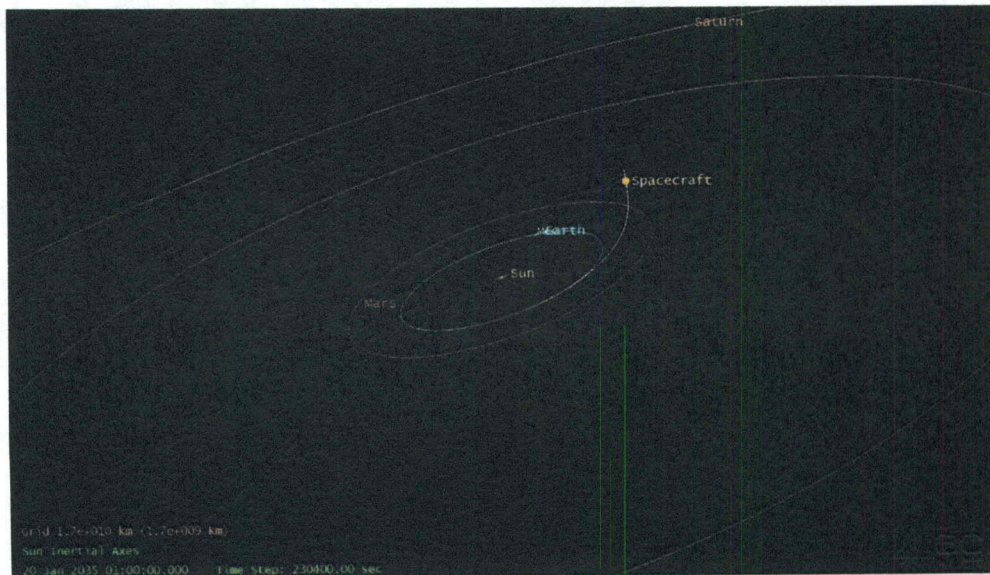


Figure 4.21 3D trajectory of spacecraft from LEO to the final HelioBurn



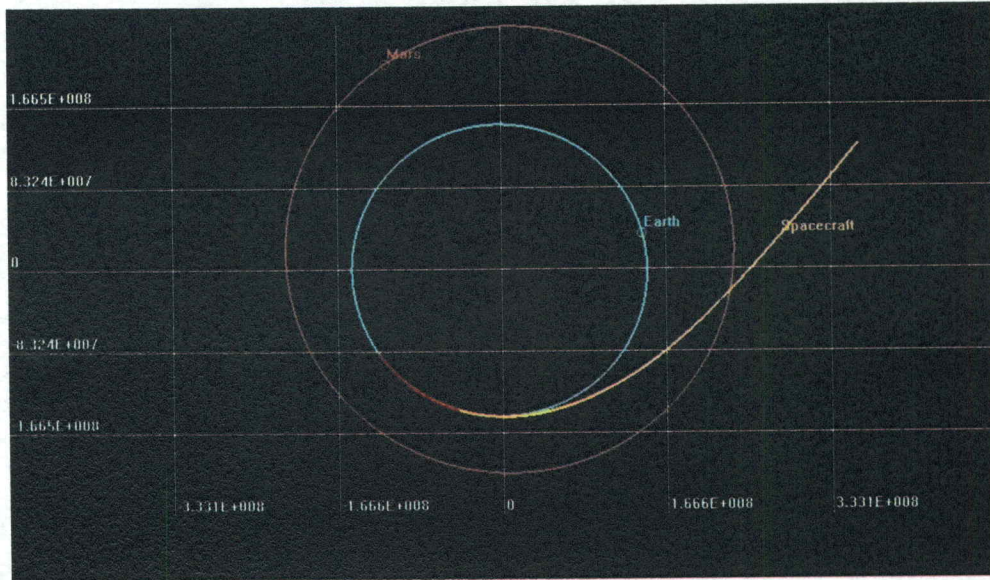


Figure 4.22 2D trajectory of spacecraft from LEO to the final Helioburn

On completion of this segment, the main thruster is turned off on 4 Feb 2034 at 17:19:22.794 UTCG. At this point, the position of the spacecraft in Sun J2000 reference frame are 117869979.62 km in X-direction, -335377986.97 km in Y-direction and -146042267.07 km in Z-direction. Thus, the magnitude distance of the spacecraft from Sun is about 384317668.10 km. Figure 4.27 shows the distance of the spacecraft from epoch to the completion of Helioburn maneuver segment in Sun J2000 reference frame.

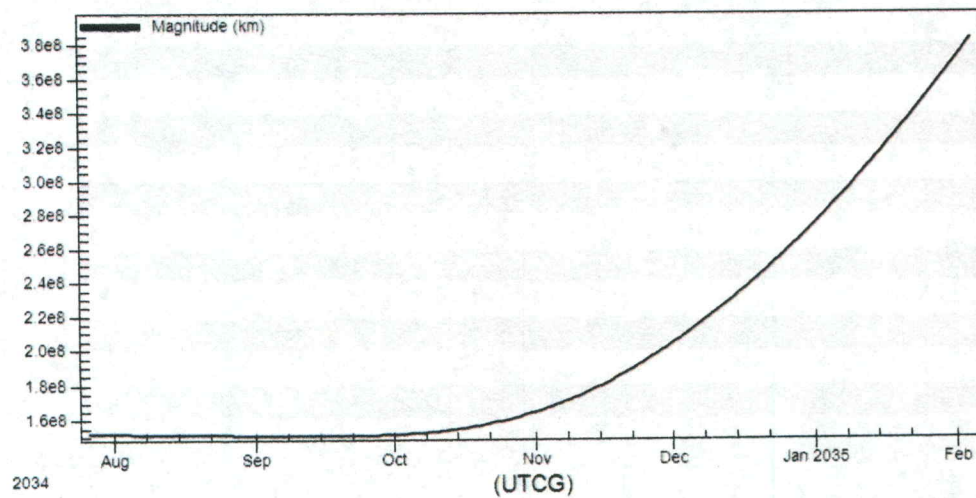


Figure 4.23 Spacecraft's distance from epoch to the final burn of Helioburn maneuver segment in Sun J2000 reference frame



The final C3 energy achieved at the end of the HelioBurn is 3040.54 km<sup>2</sup>/sec<sup>2</sup>.

Figure 4.28 shows the increment in C3 energy from epoch till the end of HelioBurn segment.

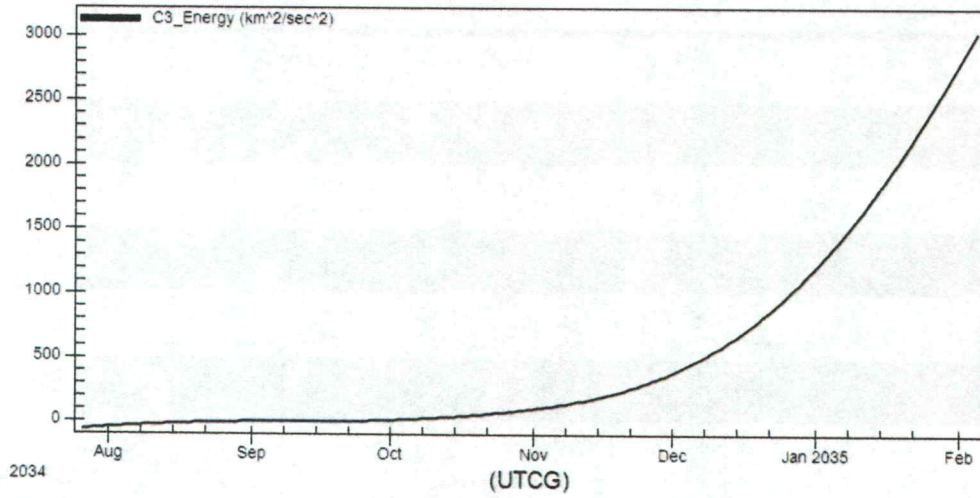


Figure 4.24 Spacecraft's C3 energy from epoch to the final burn of HelioBurn maneuver

After the completion of HelioBurn maneuver segment, the propulsion system switches from acceleration phase to coasting phase. The coasting segment is shown in Figure 4.29 and Figure 4.30.

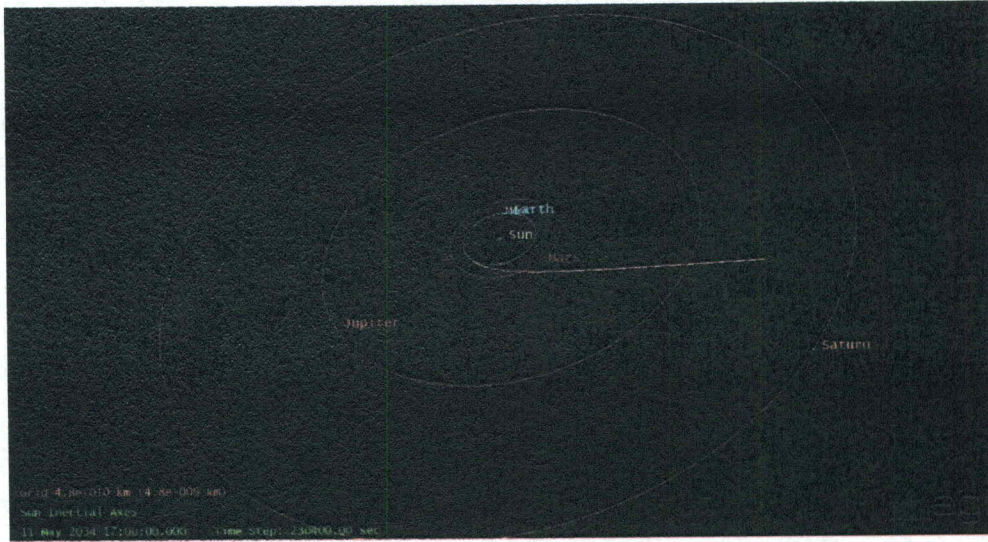


Figure 4.25 3D trajectory of spacecraft from epoch to the coasting phase

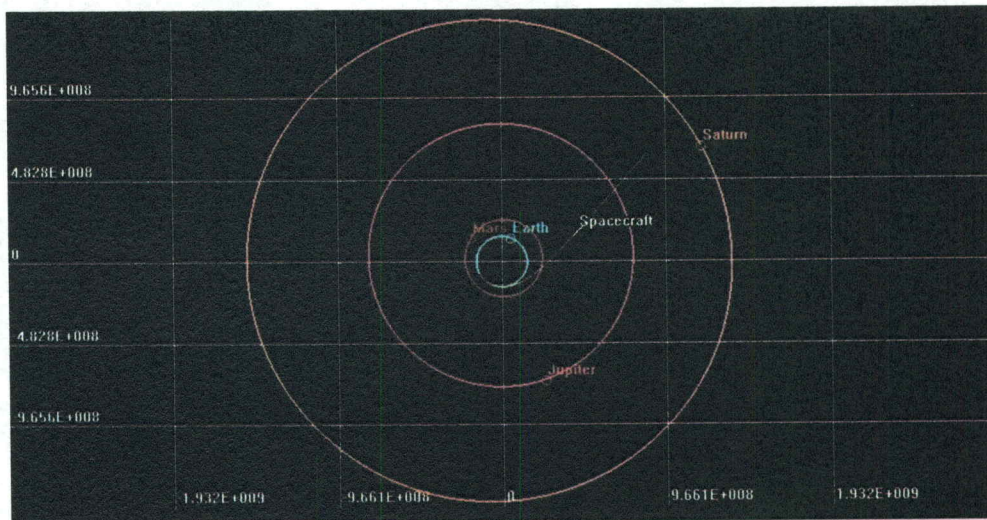


Figure 4.26 2D trajectory of spacecraft from epoch to the coasting phase

The start time for the coasting phase is on 4 Feb 2035 at 17:19:22.794 UTCG which continues till 6 Aug 2035 at 17:19:22.794 UTCG. Thus, the total duration of this phase is  $1.58 \times 10^7$  sec. After the completion of coasting phase, the spacecraft begins its maneuver segment for Saturn approach and orbit insertion phase. The spacecraft is now required to reduce its heliocentric velocity so that it can achieve orbit insertion with the help of Saturn's gravity. This requires the spacecraft to provide thrust in negative velocity vector,



which can be achieved by rotating the spacecraft in 180 degrees and continuously update the thrust vector during the propulsion system run time. Now that the spacecraft is near the Saturn's SoI, the propagator used during this maneuver segment is Saturn high precision orbit propagator which includes the third body effect of Sun, and major satellites of Saturn such as Titan, Enceladus, Mimas, Iapetus, Dione, Tethys and Rhea.

The start time for the Saturn approach phase maneuver segment is on 6 Aug 2035 at 17:19:22.794 UTCG with total duration of this segment being  $1.40 \times 10^7$  sec. The  $\Delta V$  magnitude during this segment is 42.20 km/sec and has consumed 17308.17 kg of fuel leaving 7112.29 kg of fuel left inside the main propellant tank to be used for orbit insertion and orbit correction maneuvers during the science phase of the mission. The maneuver segment for Saturn approach phase is shown in Figure 4.31 and Figure 4.32.

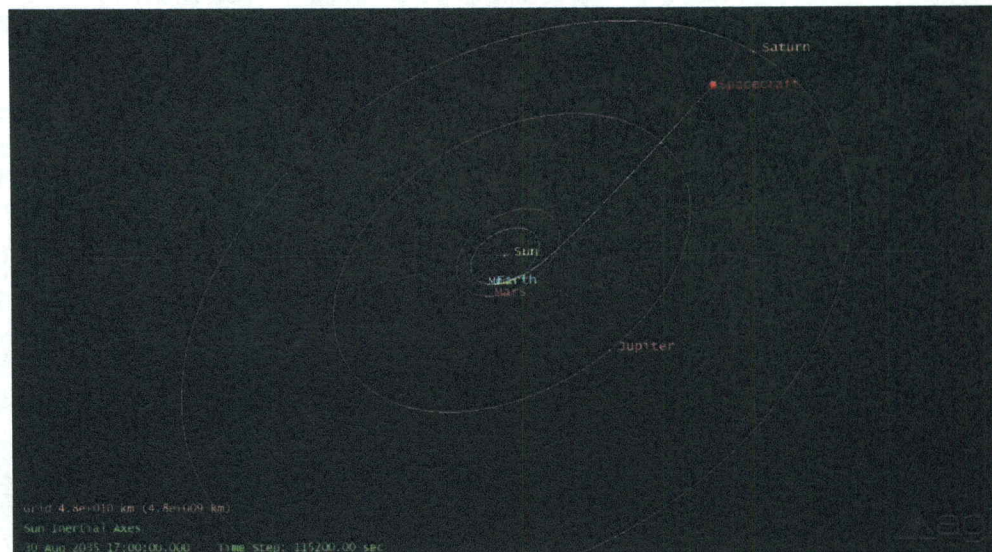


Figure 4.27 3D trajectory of spacecraft from epoch to Saturn approach phase



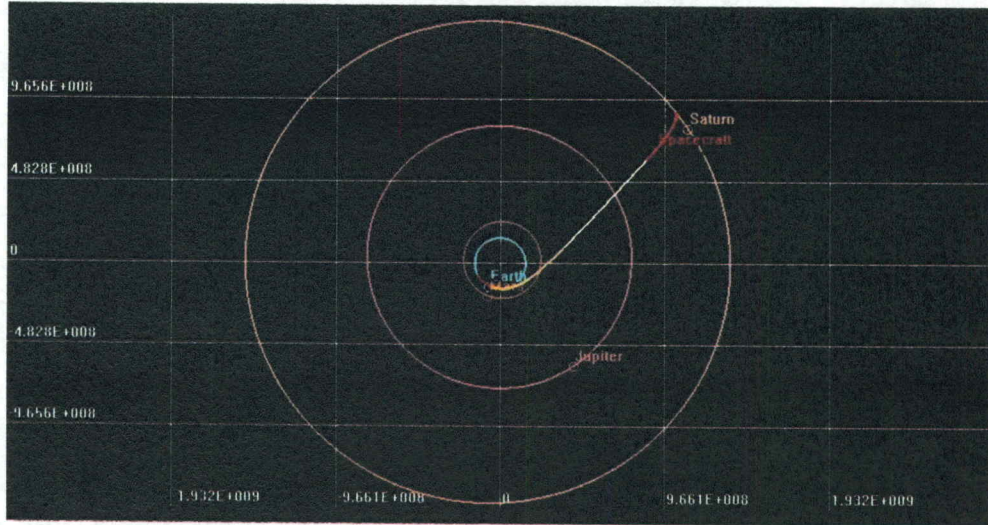


Figure 4.28 2D trajectory of spacecraft from epoch to Saturn approach

The spacecraft's captured orbit with approximate orbital period of 40 days is shown in Figure 4.33.

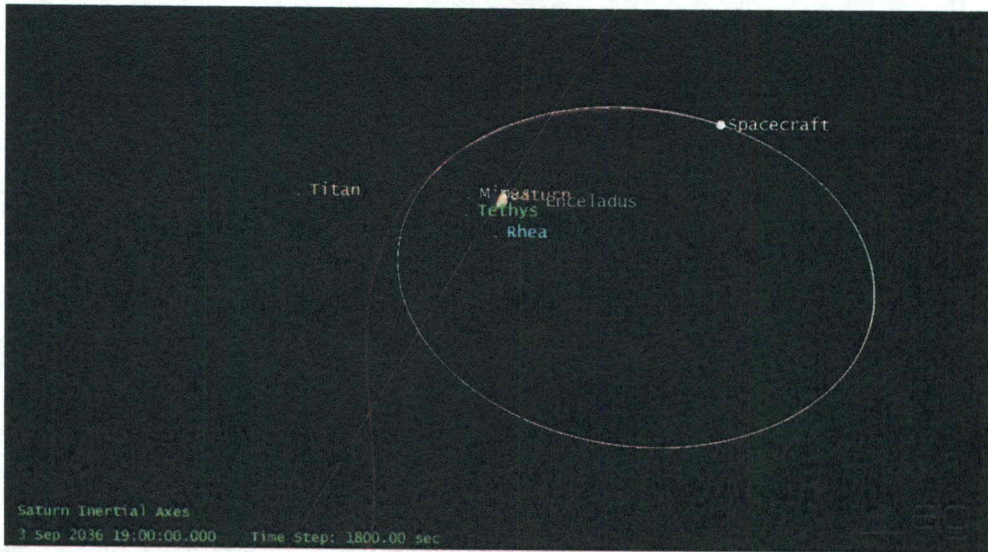


Figure 4.29 Spacecraft's captured orbit around Saturn

The spacecraft's velocity during Saturn approach phase and after orbital insertion is shown in Figure 4.34.

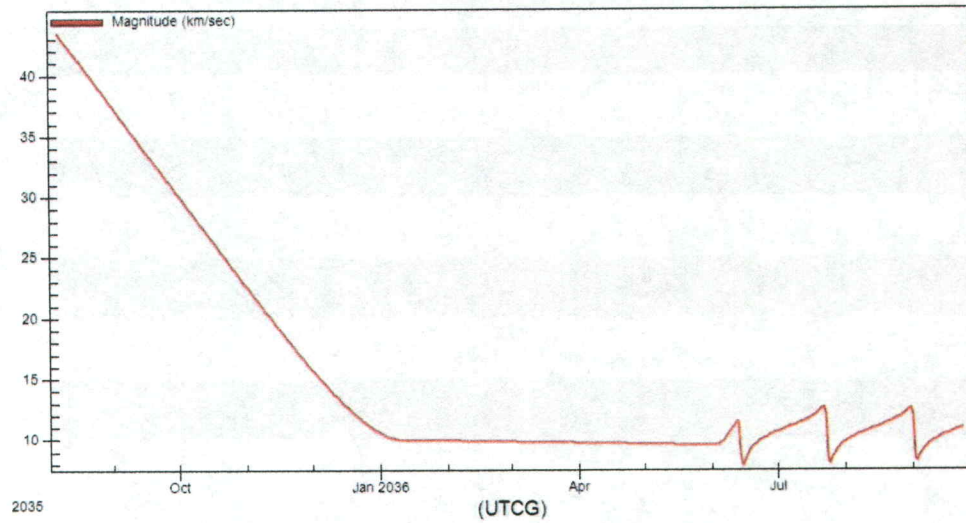


Figure 4.30 Spacecraft's velocity during Saturn approach phase and after orbital insertion

After the spacecraft has achieved the orbit capture around Saturn, a propagate segment is used to propagate the spacecraft's captured orbit for the next 100 days with Saturn's high precision orbit propagator. Finally, stop segment is used to terminate the mission. The summary of Saturn rendezvous mission timeline of is shown in table 4.9.

Table 4.9 Saturn rendezvous mission timeline

Mission Phase	Duration (days)
Initial state	0
Earth escape phase	39 days
Acceleration phase (Thrust On)	39 days
Acceleration phase (Thrust Off)	193 days
Coasting phase ends	376 days
Saturn approach phase (Thrust On)	376 days
Saturn approach phase (Thrust Off)	539 days
Coasting	679 days
Saturn orbit insertion and Orbit correction	691 days



## CHAPTER 5. COMPARISON WITH CHEMICAL AND FIELD FREE FUSION PROPULSION MISSIONS

This chapter will focus on the current and previous chemical propulsion missions to gas giant planets and compare the trip times with the previously discussed mission design using fusion propulsion system.

### 5.1 Juno Mission and Trajectory Design

The primary science goal of the Juno spacecraft is to understand the formation and evolution of planet Jupiter[80]. The spacecraft with 3.5 meters in height and 3.5 meters in diameter weights 3,625 kg at launch including 2,032 kg of fuel and oxidizer for onboard propulsion system[81]. Table 5.1 and Table 5.2 shows the spacecraft dimension and mass specifications and complete mission timeline of Juno.

Table 5.1 Juno spacecraft details

Dimensions	3.5 m high, 3.5 m diameter
Dry mass	1,593 kg
Onboard fuel	1,280 kg
Onboard oxidizer	752 kg
Total mass	3,625 kg

Table 5.2 Juno mission timeline

Mission Phase	Duration
Launch	55 hours
Inner Cruise-1	63 days
Inner Cruise-2	597 days
Deep Space Maneuver-1	~30 minutes
Deep Space Maneuver-2	~30 minutes
Earth gravity assist flyby	-
Inner Cruise-3	161 days
Outer Cruise	792 days
Jupiter approach phase	178 days
Jupiter Orbit Insertion Burn	~35 minutes
Captured orbit	53.5 days

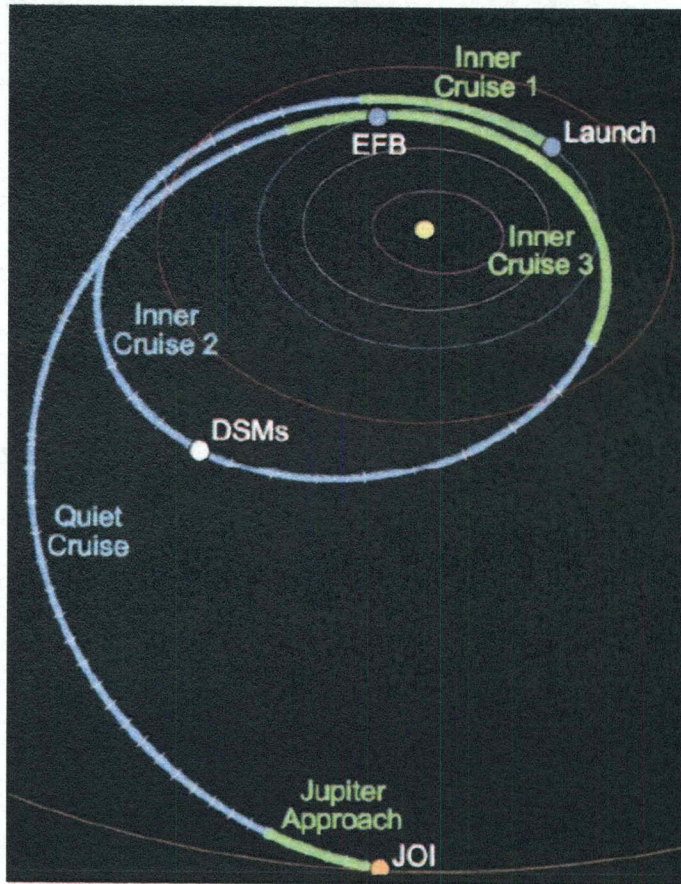


Figure 5.1 Juno's trajectory from launch to JOI.

### 5.1.1 Comparison with Juno Mission

The comparison of trip time between Juno and fusion propulsion mission show significant differences. The Juno mission reached its destination Jupiter in 1796 days from launch date of 5 Aug 2011 whereas the fusion propulsion spacecraft performs direct Jupiter rendezvous mission in 441 days from launch date of 7 Apr 2034. Thus, the fusion propulsion spacecraft takes about 24.55% of the trip time compared to Juno mission.

Due to the limitations of the launch vehicle and Juno's onboard chemical propulsion system to provide sufficient  $\Delta V$  for direct transfer to Jupiter's orbit, the spacecraft had to use an EGA trajectory. The spacecraft took about 797 days (44.32% of



the total trip time) in heliocentric orbit from launch to the EGA. The spacecraft with fusion propulsion saves time by not requiring any gravity assists.

## 5.2 Cassini-Huygens Mission and Trajectory Design

The Cassini Huygens mission was a joint science mission in collaboration with NASA, ESA and Italian Space Agency. The mission consisted of an orbiter ‘Cassini’ which had an objective to complete the first in-depth study of Saturnian system[82]. The scientific objectives of the probe ‘Huygens’ were to study the atmospheric constituents and scenarios of the evolution of Titan and its atmosphere[83]. The total mass of the spacecraft weighs 5,712 kg with adapter, fuel and Huygens probe. Table 5.4 shows the spacecraft dimension and mass specifications[84].

Table 5.3 Cassini-Huygens Spacecraft details

Dimensions	6.7 m high, 4 m width
Dry mass	2,125 kg
Huygens probe mass	320 kg
Onboard propellant	3,132 kg
Launch vehicle adapter	135 kg
Total mass	5,712 kg

The Cassini-Huygens mission was launched on 15 October 1997 at 08:43:00 UTC onboard Titan IVB launch vehicle with Centaur upper stage from Cape Canaveral, Florida. The trajectory design for Cassini to reach Saturn used VVEJGA (flybys of Venus, Venus, Earth and Jupiter gravity assist) trajectory plan. Due to the heavy mass of spacecraft, the launcher could not provide sufficient C3 energy for a direct transfer to Saturn. During the planetary alignment of Earth and Saturn in 1997, a direct transfer would have required C3

energy of  $108 \text{ km}^2/\text{s}^2$  whereas the maximum possible C3 which launch vehicle could provide was  $34 \text{ km}^2/\text{sec}^2$ . Figure 5.2 and Figure 5.3 show the trajectory of Cassini-Huygens from launch to Saturn orbit insertion phase.

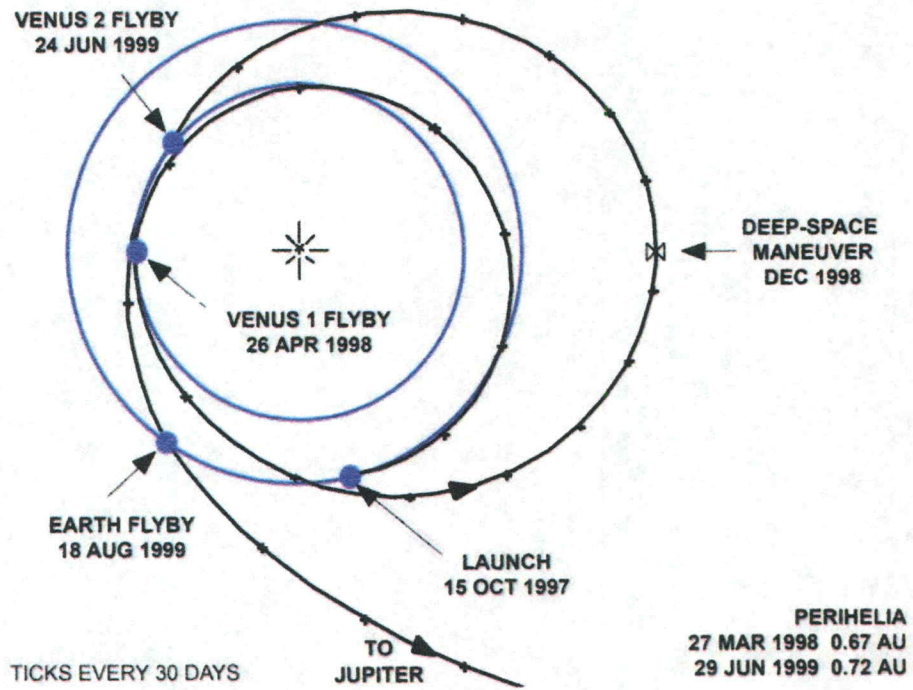


Figure 5.2 2D trajectory of Cassini-Huygens in cruise phase from epoch to Jupiter approach.

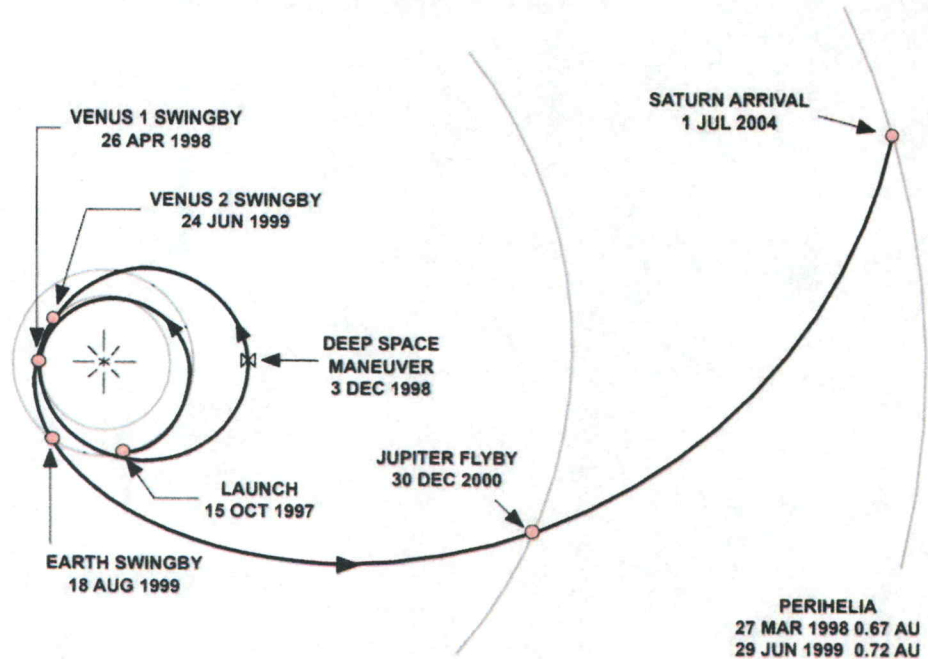


Figure 5.3 2D trajectory of Cassini-Huygens in cruise phase from epoch to Saturn orbit insertion.

### 5.2.1 Comparison with Cassini-Huygens Mission

The notable difference between the Cassini-Huygens and fusion propelled spacecraft is the total trip time. Cassini-Huygens mission shows how the spacecraft is majorly dependent on launch vehicle to provide the required  $\Delta V$  for the mission. However, a spacecraft with fusion propulsion system has the ability to provide the required  $\Delta V$  for direct transfer to Saturn. Using the VVEJGA trajectory, the Cassini-Huygens spacecraft took 2451 days from launch to Saturn's orbit insertion whereas, the fusion propulsion spacecraft takes only 691 days for a Saturn rendezvous mission. Thus, the fusion propulsion spacecraft will reach Saturn in about 28.19% of the total trip time when compared to Cassini-Huygens mission. The fusion propulsion also takes advantage of simpler direct transfer and eliminating the requirement of deep space maneuvers as compared to the complex trajectory of Cassini-Huygens involving multiple gravity assists.



### **5.3 Comparison with Field-Free Fusion Propulsion Mission**

The total trip time of the spacecraft using field-free space for a Jupiter rendezvous mission is calculated to be 336.1 days. In the field-free equations the spacecraft begins and ends its mission at zero velocity. The total distance for the Jupiter rendezvous mission is considered to be 6.20 AU (straight line distance during planetary conjunction). The trajectory analysis performed in this study shows that the spacecraft takes 446 days starting from its departure from Earth's LEO to the Jupiter's orbital insertion. The total trip time difference between field-free equation and high-fidelity trajectory analysis is of 110 days. However, it should be noted that the spacecraft takes 39 days to escape out of the Earth's gravitational influence and 40 days of coasting after obtaining Jupiter's orbital velocity. Removing this time period from the total trip times leaves us with 367 days. Thus, the spacecraft takes 367 days to reach Jupiter starting from Earth's C3 ~0 i.e., mostly during the heliocentric phase of the mission. It can be seen that the difference in trip time between field-free approximation and high-fidelity trajectory analysis is of 31 days which is under 10% of total trip time in best case scenario.

## CHAPTER 6. CONCLUSIONS AND RECOMMENDATIONS

In this thesis the complete trajectory analysis for a low thrust high specific impulse fusion propulsion system starting from Earth escape to planetary orbital insertion has been demonstrated. The conceptual mission design presented in this thesis shows that a spacecraft with nuclear fusion propulsion system can enable relatively short trip times for rendezvous missions to gas giant planets Jupiter and Saturn. The designed spacecraft has initial mass of 120 mT which fits well within the payload carrying capacity of NASA's future heavy lift launch vehicle SLS. The calculated propulsion system parameters, specific impulse of 22,500 seconds and thrust of 272 N were utilized to conduct the trajectory analysis starting from Earth escape phase, heliocentric maneuver to planetary approach and orbit insertion phase.

Most of the studies for a fusion propulsion spacecraft have concentrated towards only determining heliocentric phase or using gravity-free approximations to determine the spacecraft's total trip time. However, as this study has shown that such approximations are not very accurate and also do not highlight the complexities of Earth escape and orbital insertion phases. This study demonstrates complete mission including low thrust spiral out Earth escape, required plane changes and planetary orbital insertion methods using high-fidelity trajectory analysis. The designed direct rendezvous mission trajectory using a fusion propulsion system shows that the trip time can be reduced to about one third when compared to missions like Juno and Cassini-Huygens which utilized chemical propulsion system. The difference of total trip time with a gravity free trajectory calculation and with a high fidelity trajectory tool for Jupiter and Saturn rendezvous mission is about 110 and 285 days. This can be understood from the fact that the gravity free calculations did not

include trip time for spacecraft's departure and arrival from low orbits and planetary inclination change.

Due to the departure position of spacecraft from Earth's LEO, there is a significant amount of fuel and time required for the Earth escape maneuver. The technological and economic feasibility of spacecraft departure from Earth-Moon L1 position can be studied. There is need to further optimize the trajectory during planetary approach phase. Initially, it was decided to use a backward sequence propagation method for planetary approach phase and orbital insertion. However, after several trials the coasting and planetary approach phase did not converge successfully. Later, it was decided to use anti-velocity vector maneuver during final planetary approach phase. This method was useful to complete the rendezvous mission but required another coasting phase before orbital insertion thereby increasing trip time.

Future work should also consider the high-fidelity trajectory analysis for rendezvous missions to ice giant planets Uranus and Neptune. The feasibility of round-trip missions could also be studied to explore sample return missions to Enceladus and Titan which falls in line with the recommendation of NASA OPAG's roadmaps to the ocean world[85]. The spacecraft subsystems design and mass estimates were beyond the scope of this thesis. However, the future studies involving spacecraft design can give more emphasis on the subsystem design and mass estimates to have better understanding of the final spacecraft configuration.



## APPENDIX A

### STK ASTROGATOR USER INTERFACE AND MISSION CONTROL SEQUENCE SEGMENTS

#### A.1 User Interface

Users can define the mission sequence using the graphical programming language or using the Astrogator connect commands. The command syntax is defined in three building blocks namely, the command block, the attribute path and the attribute block. The syntax for each command is as shown below:

<Command> <Attribute Path> <Attribute>

The command block determines the location and the operation to be performed when it is executed by the user. There are three elements that define the command block.

<Prefix> {Object or scenario path} <Operator>

The attribute path defines the location of the attribute within the Astrogator module. The syntax of each attribute path depends on the attribute being executed. An example syntax of attribute path for mission control sequence is:

Astrogator \*/Spacecraft/Spacecraft1 SetValue

mainSequence.SegmentList.Propagate.<Attribute> <Value> [{Unit}]

The final block, Attribute in the Astrogator connect command identifies the attribute that the command will interact with. The syntax for attribute block is:

<Attribute> <Value> [{Unit}]

With few exceptions, most of the trajectory analysis performed in the thesis is based on the GUI based graphical programming language. Figure- 8 shows the STK/ Astrogator GUI page for Jupiter rendezvous mission.

## **A.2 Mission Control Sequence**

Each operational requirement in the trajectory design acts as a 'segment'. The segment functions as the graphical programming language in Astrogator. The Mission Control Sequence (MCS) Toolbar in Astrogator consists the buttons which define the spacecraft operation. Figure-x shows the MCS Toolbar available in Astrogator.

## **A.3 Mission Control Sequence Segments**

The MCS Segments are categorized into two types- the segments that generate ephemeris and the segments that affect the execution of MCS. The final ephemeris generated by each segment is used by the next segment to determine the trajectory accordingly. The segments that generate ephemeris are Initial State, Launch, Follow, Maneuver, Propagate, Hold and Update. The segments that affect the execution of the MCS are Sequence, Backward Sequence, Target Sequence, Return and Stop.

### **A.3.1 Initial State Segment**

The initial stage segment is used to define the initial conditions of the mission control sequence. In general, this segment specifies the spacecraft's initial condition by specifying its orbital elements, spacecraft parameters including propellant tanks.

### **A.3.2 Launch Segment**

The launch segment is the propagator for launch vehicle and can be used to model launch from any of the central bodies listed in STK. Launch segment can be used to determine the spacecraft injection and launch schedule based on the data provided by the

launch vehicle manufacturer. The parameters required to define launch segment are Central body, step size, pre-launch time, ascent type, initial acceleration, launch coordinate type and epoch, location of burnout point and burnout velocity.

### **A.3.3 Follow Segment**

The follow segment is used to set the spacecraft to follow launch vehicle with an offset and separate once the required conditions are met. This segments requires the user to define epoch, separation conditions and spacecraft's physical values.

### **A.3.4 Maneuver Segment**

The maneuver segment is used to model the spacecraft's maneuver. There are two types of maneuver's available- impulsive and finite maneuver. The impulsive maneuver uses the spacecraft's velocity vector from the previous segment and adds the  $\Delta V$  as specified by the user. The result is again sent as an output to the next MCS segment. The impulsive maneuver can be defined by the attitude,  $\Delta V$  direction and engine specification. The finite maneuver uses the propagate segment along with the thrust due to longer burn times. Finite maneuvers are more complex as it requires the segment to propagate in the defined state and account for the acceleration from the thrust. The direction of the burn is defined from the maneuvers attitude control. The finite maneuver can be defined by attitude, thrust direction, engine specifications and propagator. The spacecraft engines can be modeled based on polynomial functions for thrust and  $I_{sp}$ , custom function to determine values for propagation start, update, eval and post function. Other simpler engine models include constant thrust and  $I_{sp}$ , constant acceleration and  $I_{sp}$  and  $I_{on}$  engine models.



### **A.3.5 Propagate Segment**

The propagator segment is used to model the spacecraft's trajectory until the stopping conditions within the specified tolerance defined by the user are met. The stopping conditions can be defined using the Astrogator components which consists many conditions such as a specified target orbital parameter, delta-V etc. The segment allows the use of many numerical integrators to integrate parameters such as velocity, acceleration and constants to control the step size and accuracy of the propagation. The 7<sup>th</sup> order Runge-Kutta-Fehlberg integrator with 8<sup>th</sup> order error control is used as the default integrator to solve ordinary differential equation. Other numerical integrators available are Bulirsch-Stoer integrator based on Richardson extrapolation, 12<sup>th</sup> Gauss-Jackson integrator for second order ODE's with fixed step size, and 4<sup>th</sup> order Runge-Kutta integrator with adapting step size.

### **A.3.6 Hold Segment**

The hold segments maintains the fixed attitude and position in a reference until the stopping conditions are met. The segments holds the attitude and position and updates the ephemeris based on the time specified in step size. This segment is usually helpful for rendezvous, entry decent and landing sequences where the spacecraft is required to maintain a specific attitude or position until the next sequence can begin.

### **A.3.7 Launch Segment**

The update segment is used to modify spacecraft's properties during the mission. This segment is useful during the real time mission operations to understand the actual scenario.

### **A.3.8 Sequence Segment**

The sequence segment is used to organize the other segments and define the specified output that needs to be passed to the next segment. The sequence segment is useful when MCS has repeated segments to be executed during the mission. In that scenario, the repeated segments can be nested under sequence segment.

### **A.3.9 Backward Sequence Segment**

The backward sequence is literally the opposite of sequence segment. In this segment the nested segments are executed in backward. This sequence is helpful to determine the requirements of a desired final state of the spacecraft.

### **A.3.10 Target Sequence Segment**

The MCS segments such as maneuvers and propagators are nested under target sequence to achieve the desired result. The target sequence is defined by the search and segment configuration. The search defines the desired results requirement by the user and the segment configuration changes the segments as per the target sequences. The search profiles consist of differential corrector, interior point optimizer and sparse nonlinear optimizer. The differential corrector is used to obtain the desired results by having control parameters within the specified correction limit, perturbation value and maximum step size. The equality constraints or results are defined based on the desired output within a specified tolerance range. The iterations can be restricted by defining the maximum tolerance and convergence criteria. Newton-Raphson method or Broyden's method with specified derivative calculation method are used for root-finding algorithm. The segment configuration consist of change maneuver type, change propagator, change return segment,

change stopping condition state and seed finite maneuver. Appendix-X explains the basic differential corrector targeting algorithm.

#### **A.3.11 Return Segment**

The return segment is used to return the execution of MCS to its parent control. The segment has three states – Enable, disable and enable except when executed from target sequence segment.

#### **A.3.12 Stop Segment**

The stop segment is used to stop the MCS once the desired conditions are met or the required trajectory analysis is complete.



## APPENDIX B

### SPHERE OF INFLUENCE CALCULATIONS

The Laplace equation for the calculation of radius of sphere of influence is given by:

$$R_{SOI} = a \left( \frac{M_{ob}}{M_{pb}} \right)^{2/5} \quad (B.1)$$

where,  $R_{SOI}$  is radius of the sphere of influence of orbiting body,  $a$  is the semimajor axis of orbiting body,  $M_{ob}$  is the mass of orbiting body and  $M_{pb}$  is the mass of primary body.

Table B.1 Planetary details for SoI calculation

Celestial body	Mass, kg	Semimajor axis (a), km
Sun	$1,988,500 \times 10^{24}$	N/A
Earth	$5.97 \times 10^{24}$	$149.60 \times 10^6$
Mars	$0.642 \times 10^{24}$	$227.92 \times 10^6$
Jupiter	$1898 \times 10^{24}$	$778.57 \times 10^6$
Saturn	$568 \times 10^{24}$	$1433.53 \times 10^6$

#### D.1 Earth's Radius of Sphere of Influence

$$R_{SOI} = 149.60 \times 10^6 \left( \frac{5.97 \times 10^{24}}{1.98 \times 10^{30}} \right)^{2/5} = 924,526 \text{ km}$$

### D.2 Jupiter's Radius of Sphere of Influence

$$R_{SOI} = 778.57 \times 10^6 \left( \frac{1898 \times 10^{24}}{1.98 \times 10^{30}} \right)^{2/5} = 48.2 \times 10^6 \text{ km}$$

### D.3 Saturn's Radius of Sphere of Influence

$$R_{SOI} = 1433.53 \times 10^6 \left( \frac{568 \times 10^{24}}{1.98 \times 10^{30}} \right)^{2/5} = 54.6 \times 10^6 \text{ km}$$

## REFERENCES

- [1] Y. Guo and R. W. Farquhar, “New Horizons Mission Design,” in *New Horizons*, Springer, New York, NY, 2009, pp. 49–74.
- [2] Y. Guo and R. W. Farquhar, “New Horizons Pluto–Kuiper Belt mission: design and simulation of the Pluto–Charon encounter,” *Acta Astronautica*, vol. 56, no. 3, pp. 421–429, Feb. 2005.
- [3] E. Stone, L. Alkalai, and L. Friedman, “Science and Enabling Technologies for the Exploration of the Interstellar Medium,” 2015.
- [4] S. Oleson and S. Benson, “Radioisotope Electric Propulsion for Fast Outer Planetary Orbiters,” in *38th AIAA/ASME/SAE/ASEE Joint Propulsion Conference & Exhibit*, American Institute of Aeronautics and Astronautics.
- [5] S. Oleson *et al.*, *Outer Planet Exploration With Advanc Radioisotope Electric Propulsion ed.* 2002.
- [6] P. Janhunen, “Electric Sail for Spacecraft Propulsion,” *Journal of Propulsion and Power*, vol. 20, no. 4, pp. 763–764, 2004.
- [7] G. Mengali, A. A. Quarta, and P. Janhunen, “Electric Sail Performance Analysis,” *Journal of Spacecraft and Rockets*, vol. 45, no. 1, pp. 122–129, 2008.
- [8] C. R. McInnes, *Solar Sailing: Technology, Dynamics and Mission Applications*. Berlin Heidelberg: Springer-Verlag, 2004.
- [9] C. G. Sauer, “Solar sail trajectories for solar polar and interstellar probe missions,” *Astrodynamics*, pp. 547–562, 1999.
- [10] R. Frisbee and S. Leifer, “Evaluation of propulsion options for interstellar missions,” in *34th AIAA/ASME/SAE/ASEE Joint Propulsion Conference and Exhibit*, American Institute of Aeronautics and Astronautics.
- [11] L. Johnson and S. Leifer, “Propulsion options for interstellar exploration,” in *36th AIAA/ASME/SAE/ASEE Joint Propulsion Conference and Exhibit*, American Institute of Aeronautics and Astronautics.
- [12] J. Cassibry *et al.*, “Case and Development Path for Fusion Propulsion,” *Journal of Spacecraft and Rockets*, vol. 52, no. 2, pp. 595–612, 2015.
- [13] “Systems Tool Kit,” *Agi*. [Online]. Available: <http://www.agi.com/products/engineering-tools>. [Accessed: 17-Feb-2018].
- [14] K. E. Tsiolkovskiy, “Study of Outer Space by Reaction Devices,” *NASA Technical Translation, NASA TT F-15571*, p. 742.
- [15] M. Meyer, L. Johnson, B. Palaszewski, D. Goebel, H. White, and D. Coote, “In-Space Propulsion Systems Roadmap Technology Area 02,” National Aeronautics and Space Administration, Office of the Chief Technologist, Apr. 2012.
- [16] G. P. Sutton and O. Biblarz, *Rocket Propulsion Elements*. John Wiley & Sons, 2010.
- [17] R. G. Jahn, *Physics of Electric Propulsion*. Courier Corporation, 2006.
- [18] W. J. E. Jr, *Principles of Nuclear Rocket Propulsion*. Butterworth-Heinemann, 2016.
- [19] G. Vulpetti, L. Johnson, and G. L. Matloff, *Solar Sails: A Novel Approach to Interplanetary Travel*. Springer, 2014.
- [20] D. L. Gallagher, L. Johnson, J. Moore, and F. Bagenal, *Electrodynamic Tether Propulsion and Power Generation at Jupiter*. .
- [21] J. C. Mankins, “Technology readiness levels, A White Paper,” NASA, Washington, DC, Apr. 1995.



- [22] R. H. Frisbee, "Advanced Space Propulsion for the 21st Century," *Journal of Propulsion and Power*, vol. 19, no. 6, pp. 1129–1154, 2003.
- [23] E. W. Davis, "Advanced Propulsion Study," WARP DRIVE METRICS LAS VEGAS NV, WARP DRIVE METRICS LAS VEGAS NV, Feb. 2004.
- [24] T. Kammash, *Fusion energy in space propulsion*. Washington, DC: American Institute of Aeronautics and Astronautics, 1995.
- [25] S. Atzeni and J. Meyer-ter-Vehn, *The Physics of Inertial Fusion: Beam-Plasma Interaction, Hydrodynamics, Hot Dense Matter*. Clarendon Press, 2004.
- [26] K. Ikeda, "Progress in the ITER Physics Basis," *Nucl. Fusion*, vol. 47, no. 6, 2007.
- [27] T. J. McGuire and R. J. Sedwick, "Improved Confinement in Inertial Electrostatic Confinement for Fusion Space Power Reactors," *Journal of Propulsion and Power*, vol. 21, no. 4, pp. 697–706, Jul. 2005.
- [28] I. R. Lindemuth, "The ignition design space of magnetized target fusion," *Physics of Plasmas*, vol. 22, no. 12, p. 122712, Dec. 2015.
- [29] C. D. Orth, "Overview of the VISTA Spacecraft Concept Powered by Inertial Confinement Fusion," Lawrence Livermore National Lab. (LLNL), Livermore, CA (United States), UCRL-JC-141514, Nov. 2000.
- [30] E. I. Moses, "The National Ignition Facility and the Promise of Inertial Fusion Energy," *FST*, vol. 60, no. 1, pp. 11–16, Jul. 2011.
- [31] R. Aymar, P. Barabaschi, and Y. Shimomura, "The ITER design," *Plasma Phys. Control. Fusion*, vol. 44, no. 5, p. 519, 2002.
- [32] S. A. Slutz *et al.*, "Scaling magnetized liner inertial fusion on Z and future pulsed-power accelerators," *Physics of Plasmas*, vol. 23, no. 2, p. 022702, Feb. 2016.
- [33] G. A. Wurden *et al.*, "Magneto-Inertial Fusion," *J Fusion Energ*, vol. 35, no. 1, pp. 69–77, Feb. 2016.
- [34] Brian. Riehm, "Preliminary trajectory analysis of a nuclear fusion propulsion fly-by mission to Saturn and beyond: a thesis," Thesis MSE -- University of Alabama in Huntsville, 2012.
- [35] J. F. Dugan and C. R. Simsic, "Analysis of Trajectory Parameters for Probe and Round-Trip Missions to Venus," National Aeronautics and Space Administration, TN D-470, Nov. 1960.
- [36] K. M. Carlson, "An Analytical Solution to Patched Conic Trajectories Satisfying Initial and Final Boundary Conditions," Nov. 1970.
- [37] M. Kim, "Continuous low-thrust trajectory optimization: Techniques and applications," Virginia Tech, 2005.
- [38] C. Sauer Jr., "A Preliminary User's Guide to VARITOP, SAIL and SEPTOP General Purpose Low-Thrust Trajectory Optimization Programs," Jet Propulsion Laboratory, Pasadena, CA, Feb. 2002.
- [39] "Mission design for deep space 1: A low-thrust technology validation mission - ScienceDirect." [Online]. Available: <https://www.sciencedirect.com/science/article/pii/S0094576599001575>. [Accessed: 15-Mar-2018].
- [40] R. B. Adams *et al.*, "Conceptual Design of In-Space Vehicles for Human Exploration of the Outer Planets," Nov. 2003.
- [41] Philip G. Hill, *Mechanics and thermodynamics of propulsion*. Reading, Mass.: Addison-Wesley PubCo, 1965.



- [42] C. H. D. Williams, "Realizing '2001: A Space Odyssey': Piloted Spherical Torus Nuclear Fusion Propulsion," NASA John H. Glenn Research Center, NASA/TM-2005-213559, Mar. 2005.
- [43] C. H. Williams, "An Analytic Approximation to Very High Specific Impulse and Specific Power Interplanetary Space Mission Analysis," presented at the Space Flight Mechanics Meeting, 11-15 1996, United States, 1995.
- [44] C. H. Williams, L. A. Dudzinski, S. K. Borowski, and A. J. Juhasz, "Realizing '2001: A Space Odyssey': Piloted Spherical Torus Nuclear Fusion Propulsion," *Journal of Spacecraft and Rockets*, vol. 39, no. 6, pp. 874–885, 2002.
- [45] C. D. Orth, "VISTA -- A Vehicle for Interplanetary Space Transport Application Powered by Inertial Confinement Fusion," Lawrence Livermore National Lab., UCRL-TR--110500, 2005.
- [46] N. R. Schulze, "Fusion energy for space missions in the 21st Century," Aug. 1991.
- [47] R. B. Adams, J. T. Cassibry, and K. Schillo, "Developing the Pulsed Fission-Fusion (PuFF) Engine," in *50th AIAA/ASME/SAE/ASEE Joint Propulsion Conference*, American Institute of Aeronautics and Astronautics.
- [48] T. Polsgrove *et al.*, "Design of Z-pinch and Dense Plasma Focus Powered Vehicles," in *49th AIAA Aerospace Sciences Meeting including the New Horizons Forum and Aerospace Exposition*, American Institute of Aeronautics and Astronautics.
- [49] J. Miernik *et al.*, "Z-Pinch fusion-based nuclear propulsion," *Acta Astronautica*, vol. 82, no. 2, pp. 173–182, Feb. 2013.
- [50] T. R. Jarboe *et al.*, "Spheromak Fusion Propulsion for Future Solar System Exploration," *Journal of Propulsion and Power*, vol. 21, no. 2, pp. 218–229, 2005.
- [51] J. Carrico and E. Fletcher, "Software Architecture and Use of Satellite Tool Kit's Astrogator Module for Libration Point Orbit Missions," in *Libration Point Orbits and Applications*, World Scientific, 2003, pp. 471–487.
- [52] N. Murakami and K. Yamanaka, "Trajectory design for rendezvous in lunar Distant Retrograde Orbit," in *2015 IEEE Aerospace Conference*, 2015, pp. 1–13.
- [53] J. D. Strizzi, J. M. Kutrieb, P. E. Damphousse, and J. P. Carrico, "Sun-Mars Libration Points and Mars Mission Simulations," 2001.
- [54] T. R. Kulkarni and D. Mortari, "Low energy interplanetary transfers using halo orbit hopping method with STK/Astrogator," *Advances in the Astronautical Sciences*, no. 120, pp. 155–168, 2005.
- [55] C. Nickel, J. P. Carrico Jr., R. Lebois, L. Policastri, and R. Sherman, "LADEE Flight Dynamics System Overview," *Proceedings of the 25th AAS/AIAA Space Flight Mechanics Meeting*, Jan. 2015.
- [56] D. W. Dunham *et al.*, "Transfer trajectory design for the SOHO libration-point mission," presented at the Washington, DC International Astronautical Federation Congress, 1992.
- [57] C. E. Roberts, "Long duration Lissajous orbit control for the ACE Sun-Earth L 1 Libration Point Mission," in *Proceeding of the 11th Annual AAS/AIAA Space Flight Mechanics Meeting, Santa Barbara, CA, Feb. 11-15, 2001*, 2001, vol. 2, pp. 1447–1464.
- [58] M. M. Berry and L. M. Healy, "Implementation of Gauss-Jackson Integration for Orbit Propagation," 2004.



- [59] F. R. Hoots and R. G. France, "An Analytic Satellite theory using gravity and a dynamic atmosphere," *Celestial Mechanics*, vol. 40, no. 1, pp. 1–18, 1987.
- [60] J. J. F. Liu and R. L. Alford, "Semianalytic theory for a close-Earth artificial satellite," *Journal of Guidance, Control, and Dynamics*, vol. 3, no. 4, pp. 304–311, 1980.
- [61] J. G. Neelon, "Current development of the draper semianalytical satellite theory standalone orbit propagator package," *Astrodynamics*, pp. 2037–2051, 1997.
- [62] D. J. Fonte, B. Neta, C. Sabol, D. A. Danielson, and W. R. Dyar, "Comparison of Orbit Propagators in the Research and Development Goddard Trajectory Determination System (R & D GTDS). Part I: Simulated Data," Aug. 1995.
- [63] C. A. Jablonski, "Application of Semianalytic Satellite Theory to Maneuver Planning," AIR FORCE INST OF TECH WRIGHT-PATTERSON AFB OH, AIR FORCE INST OF TECH WRIGHT-PATTERSON AFB OH, AFIT/CI/CIA-91-049, May 1991.
- [64] S. J. Setty, P. J. Cefola, O. Montenbruck, and H. Fiedler, "Application of Semi-analytical Satellite Theory orbit propagator to orbit determination for space object catalog maintenance," *Advances in Space Research*, vol. 57, no. 10, pp. 2218–2233, May 2016.
- [65] "Department of Defence World Geodetic System 1984," national Imagery and Mapping Agency, TR8350.2.
- [66] A. S. Konopliv, S. W. Asmar, E. Carranza, W. L. Sjogren, and D. N. Yuan, "Recent Gravity Models as a Result of the Lunar Prospector Mission," *Icarus*, vol. 150, no. 1, pp. 1–18, Mar. 2001.
- [67] F. G. Lemoine *et al.*, "An improved solution of the gravity field of Mars (GMM-2B) from Mars Global Surveyor," *J. Geophys. Res.*, vol. 106, no. E10, pp. 23359–23376, Oct. 2001.
- [68] R. A. Jacobson, "JUP230 orbit solution." NASA Tech. Memorandum, 2003.
- [69] R. A. Jacobson, "The Orbits of the Major Saturnian Satellites and the Gravity Field of Saturn from Spacecraft and Earth-based Observations," *AJ*, vol. 128, no. 1, p. 492, 2004.
- [70] R. A. Jacobson, "The Orbits of the Uranian Satellites and Rings, the Gravity Field of the Uranian System, and the Orientation of the Pole of Uranus," *AJ*, vol. 148, no. 5, p. 76, 2014.
- [71] R. A. Jacobson, "The Orbits of the Neptunian Satellites and the Orientation of the Pole of Neptune," *AJ*, vol. 137, no. 5, p. 4322, 2009.
- [72] D. Conte and D. B. Spencer, "Targeting the martian moons via direct insertion into mars-orbit," in *Astrodynamics 2015*, 2016, pp. 2389–2406.
- [73] P. K. Seidelmann, "1980 IAU Theory of Nutation: The final report of the IAU Working Group on Nutation," *Celestial Mechanics*, vol. 27, no. 1, pp. 79–106, May 1982.
- [74] E. Hairer, S. P. Nørsett, and G. Wanner, *Solving Ordinary Differential Equations I: Nonstiff Problems*, 2nd ed. Berlin Heidelberg: Springer-Verlag, 1993.
- [75] K. F. Robinson, K. Hefner, and D. Hitt, "NASA's Space Launch System: An Evolving Capability for Exploration," presented at the 9th IAA Symposium on the future of space exploration: Towards new global programmes, Torino, Italy, 2015.



- [76] A. Jackman, "NASA'S Space Launch System: Progress Toward the Proving Ground," presented at the 10th IAA Symposium on the Future of Space Exploration 2017, 27-29 Jun. 2017, Italy, 2017.
- [77] W. E. Moeckel, "Comparison of advanced propulsion concepts for deep space exploration," *Journal of Spacecraft and Rockets*, vol. 9, no. 12, pp. 863–868, 1972.
- [78] "NASA GSFC Jupiter Fact Sheet." [Online]. Available: <https://nssdc.gsfc.nasa.gov/planetary/factsheet/jupiterfact.html>. [Accessed: 28-Feb-2018].
- [79] "NASA GSFC Saturn Fact Sheet." [Online]. Available: <https://nssdc.gsfc.nasa.gov/planetary/factsheet/saturnfact.html>. [Accessed: 28-Feb-2018].
- [80] R. S. Grammier, "A look inside the Juno Mission to Jupiter," in *2009 IEEE Aerospace conference*, 2009, pp. 1–10.
- [81] "Juno Launch Press Kit." National Aeronautics and Space Administration, Aug-2011.
- [82] D. L. Matson, L. J. Spilker, and J.-P. Lebreton, "The Cassini/Huygens Mission to the Saturnian System," *Space Science Reviews*, vol. 104, no. 1–4, pp. 1–58, Jul. 2002.
- [83] J.-P. Lebreton and D. L. Matson, "The Huygens Probe: Science, Payload and Mission Overview." [Online]. Available: <http://adsabs.harvard.edu/full/1997ESASP1177...5L>. [Accessed: 02-Mar-2018].
- [84] "Cassini Launch press Kit." National Aeronautics and Space Administration, Oct-1997.
- [85] A. Hendrix and T. Hurford, "Ocean Worlds: Priorities, Missions Scenarios, & Technologies," NASA OPAG, Feb. 2018.